Am J Transl Res 2026;18(5):3765-3782
www.ajtr.org /ISSN:1943-8141/AJTR0172175

Original Article

Plasma ECRG4 as a novel diagnostic marker for Alzheimer's disease associated with oligodendrocyte dysfunction

Lifu Zhang[1], Naoki Ikeda[1], Shuji Takeda[2], Naoto Oikawa[1], Shigeo Murayama[3], Uichi Koshimizu[2], Ichiro Yabe[4], Toru Kondo[1]

[1]Division of Stem Cell Biology, Institute for Genetic Medicine, Hokkaido University, Sapporo, Hokkaido 060-0815, Japan; [2]ASUBIO Pharma Co., Ltd., Kobe, Hyogo 650-0047, Japan; [3]Department of Neuropathology, Brain Bank for Aging Research, Tokyo Metropolitan Institute of Gerontology, Itabashi-ku, Tokyo 173-0015, Japan; [4]Department of Neurology, Faculty of Medicine and Graduate School of Medicine, Hokkaido University, Sapporo, Hokkaido 060-8638, Japan

Received February 19, 2026; Accepted April 16, 2026; Epub May 15, 2026; Published May 30, 2026

Abstract: Current treatments for Alzheimer's disease (AD) primarily focus on slowing disease progression, emphasizing the urgent need for a reliable diagnostic method for early-stage Alzheimer's (EAD). Our investigation, which is based on the finding that the secretory protein Esophageal Cancer Related Gene 4 (ECRG4) is elevated in the hippocampus of AD patients, led to the creation of a novel ELISA system for ECRG4 detection. We observed that ECRG4 peptides, particularly the fragment spanning amino acids 108-132, were elevated in the plasma of approximately 25% of patients with mild cognitive impairment (MCI) and 50% of those with AD, compared to individuals without dementia. RNA sequencing of plasma samples revealed decreased levels of carbohydrate sulfotransferase 3 (*CHST3*) mRNA, which is mainly expressed in oligodendrocyte (OLG)-lineage cells, in ECRG4-positive patients. Functional analyses demonstrated that the ECRG4 (71-107) peptide induced cytotoxicity in oligodendrocytes in vitro and reduced the expression of the OLG marker galactocerebroside in the corpus callosum following intracerebral injection. Additionally, peptide injection resulted in extravascular IgG leakage and the accumulation of OLG precursor cells (OPCs), which are crucial for myelin regeneration, around the blood vessels. These phenomena were similarly observed in the hippocampi of patients with EAD. Collectively, these findings establish ECRG4 as a novel serum marker for AD and suggest its association with ECRG4-dependent OLG dysfunction.

Keywords: ECRG4, ELISA, plasma, Alzheimer's disease, oligodendrocyte

Introduction

The development of Alzheimer's disease (AD) involves multiple pathological changes, including the accumulation of hyperphosphorylated tau proteins, formation of neurofibrillary tangles, and neurovascular dysfunction [1-3]. Notably, amyloid-β (Aβ) plaques begin to accumulate during the early stage of AD (EAD). Understanding the molecular mechanisms underlying brain plaque formation is essential for the development of effective preventive strategies [4]. Recently, two therapeutic antibodies, donanemab and lecanemab, have been developed to target these plaques [5, 6], and have received marketing authorization from the U.S. Food and Drug Administration (FDA). However, their therapeutic efficacy is primarily confined to patients with mild cognitive impairment (MCI) or EAD, highlighting an urgent need for novel diagnostic methods capable of accurately identifying these populations.

Esophageal cancer related gene 4 (ECRG4, or Augurin), was initially identified as a gene significantly downregulated in malignant tumors compared to adjacent normal tissues [7, 8]. Overexpression of ECRG4 has been reported to trigger cell cycle arrest in tumor cells *in vitro* [9], establishing ECRG4 as a tumor suppressor gene. In contrast, increased ECRG4 expression has been observed in the brains of aged mice

https://doi.org/10.62347/GBUB6697

and in the hippocampus of AD patients carrying the apolipoprotein E (APOE) 3/4 genotype, compared to patients with the APOE3/3 genotype and non-AD controls [10-12]. In addition, we observed focal upregulation of ECRG4 in the hippocampus of patients with EAD and AD across APOE 3/3, 3/4, and 4/4 genotypes, along with its colocalization with amyloid precursor protein (APP)/Aβ in the same regions (Lai Kit et al, unpublished data). Furthermore, ECRG4 stimulates the activation of inflammatory cytokine cascades, including tumor necrosis factor-α (TNF-α) and interleukin-6 (IL-6), in microglia, thereby contributing to both AD development and tumor rejection [13-15]. Collectively, these observations imply that that ECRG4 may serve as a novel diagnostic marker for the detection of EAD and MCI. Given that ECRG4 is a secreted protein that can be cleaved by specific proteases, including furin and thrombin [16-18], we hypothesized that certain ECRG4 fragments may be detectable in the body fluids, such as blood and cerebrospinal fluid (CSF) in patients with MCI, EAD, or AD. For this purpose, we constructed a highly sensitive enzyme-linked immunosorbent assay (ELISA) targeting the ECRG4 peptide fragment spanning amino acids 108-132.

Methods

Chemical reagents

Chemicals were obtained from Nacalai Tesque and Sigma-Aldrich unless otherwise specified.

Ethical approval

This study was conducted in accordance with the Declaration of Helsinki and was approved by the Ethics Committee of Tokyo Metropolitan Institute for Geriatrics and Gerontology (Protocol code: R2, Date of approval: April 15, 2019), the Ethics Committee of Hokkaido University Graduate School of Medicine (Protocol code: 16-031, Date of approval: July 16, 2018), and the Ethics Committee of Hokkaido University Institute for Genetic Medicine (Protocol code: 12-0001(6), Date of approval: December 21, 2021). The protocol for animal study was approved by the Institutional Review Board of the Animal Care and Use Committee of Hokkaido University (Protocol code: 21-0066, Date of approval: July 19, 2021).

Animals

C57BL/6 and NOD/ShiJic-scid (NOD/SCID) mice were purchased from CLEA Japan. A three-drug anesthetic mixture comprising medetomidine hydrochloride (0.3 mg/kg, M3314, Tokyo Chemical Industry), midazolam (4 mg/kg, 135-13791, FUJIFILM Wako), and butorphanol tartrate (5 mg/kg, 021-19001, FUJIFILM Wako) was used in the animal experiments. The anesthetic mixture was administered via intraperitoneal injection at a volume of 0.1 ml per 10 g body weight. For euthanasia, pentobarbital sodium (150 mg/kg, 76-74-4, FUJIFILM Wako) was administered intraperitoneally at a volume of 0.1 ml per 10 g body weight.

Mice were housed under controlled conditions. The temperature was maintained at 24 ± 2°C. The relative humidity was maintained between 0% and 20%. A 12 h light/12 h dark cycle was implemented, with lights on from 6:00 a.m. to 6:00 p.m. Mice were provided with a standardized commercial diet (Labo MR Stock, Nosan Corporation) and had ad libitum access to water supplied through bottles placed on the cage lids. Paper-based bedding (Paper Clean, SLC) was used and replaced regularly to maintain hygienic conditions.

Anti-ECRG4 antibodies

A rabbit polyclonal anti-ECRG4 antibodies (Abs) (OB1264) were produced by immunizing a Japanese White rabbit with a synthetic peptide corresponding to amino acids 107-132 (CRNRNGHDYYGDYYQRHYDEDAAIGPH) using a standard protocol (Medical & Biological Laboratories) (Figure S1A).

Mouse monoclonal anti-ECRG4 Abs were produced by immunizing C57BL/6 mice with a mixture of GST-AUGURIN expressed in *E. coli* and a 21-mer peptide derived from the N-terminus of AUGURIN. The epitopes of each monoclonal antibody were determined using a peptide SPOT array synthesized by Multipep (CEM) (Figure S1A). After intraperitoneal injection of hybridoma cells (clones 3B4, 2A8, 1H4, and 1A3; 5×10^6) into NOD/SCID mice (8-week-old), the ascites were collected. Both mouse and rabbit anti-ECRG4 Abs were purified using Protein A Sepharose 4 Fast Flow according to the manufacturer's protocol (17-5280-01, GE Healthcare).

Diagnosis of dementia, AD, and non-dementia

Patients were diagnosed with dementia, AD, and MCI in accordance with established guidelines and the National Institute on Aging-Alzheimer's Association (NIA-AA) criteria (Table S1) [19, 20]. For inclusion criteria, probable AD was defined based on the NINCDS-ADRDA criteria, and MCI was diagnosed according to Petersen's criteria [21]. Cases with clear co-occurring central nervous system disorders, such as head trauma, cerebrovascular disease, or other neurodegenerative diseases (e.g., Parkinson's disease), were excluded. Non-dementia patients with other neurological disorders were classified according to the criteria specified in Table S2. The Mini-Mental State Examination (MMSE) was used for dementia diagnosis [19, 20].

Human plasma, cerebrospinal fluid, and hippocampal sections

EDTA-treated plasma (plasma) and CSF samples were collected using standard procedures from three patient groups: (i) patients with dementia, including AD and normal pressure hydrocephalus, (ii) individuals with MCI, and (iii) individuals with non-dementia neurological diseases (e.g., multiple system atrophy and myopathy) [20, 21]. Plasma samples from eight healthy individuals were used as controls. Hippocampal tissues were obtained from patients diagnosed with non-AD, EAD, or AD, as previously documented [22].

ECRG4 sandwich ELISA assay

A mouse anti-ECRG4 antibody (1 μg/mL in carbonate buffer [0.05 M, pH 9.5], 37116-08 and 37141-08, Kanto Chemical) was used to coat 96-well plates (353072, Falcon), followed by overnight incubation at 4°C. After washing five times with washing buffer (0.05% Tween-20/PBS; JP-0777A and 049-29793, FUJIFILM Wako), the plates were incubated with blocking buffer (5% skim milk in carbonic acid buffer; 190-12865, FUJIFILM Wako) for 90 min at room temperature (RT). After three additional washes with the washing buffer, 50 μl of samples were added to each well. These included ECRG4 peptide (AUGRIN precursor [71-148] and prepro-AUGRIN [71-132] as positive controls, 1 ng/mL; 012-25A and 012-26A, Phoenix Pharmaceuticals), plasma (diluted 1:2), and CSF (diluted 1:2), all prepared in assay buffer (2.5% skim milk in washing buffer). The plates were then incubated for 90 min at RT.

After five washes, the wells were incubated with primary antibody OB1264 (1 μg/ml in assay buffer) for 60 min at RT. Subsequently, following three washes, the wells were incubated in the dark with goat anti-rabbit IgG-HRP (1:1000, 1706515, Bio-Rad) diluted in assay buffer for 60 min at RT. After five washes, TMB substrate solution (5120-0077, KPL) was added and incubated in the dark for 30 min at RT. The reaction was stopped by adding sulfuric acid, and the absorbance was measured at 450 nm using a Benchmark microplate reader (170-6750, Bio-Rad). The optimal concentrations of the capture and detection antibodies were determined experimentally (Figure S1B, S1C).

The standard curve was described by the equation: $y = 0.0723x + 0.0323$, where y denotes the signal intensity and x represents the peptide concentration. Based on a background signal of 0.05, the limit of quantification was approximately 0.25 μg/mL.

Expression vectors

Mouse Ecrg4 fragments (amino acids 32-70 and 71-132) were amplified from pCMS-EGFP-mEcrg4 [11] using KOD plus-Ver.2 DNA polymerase in accordance with the supplier's guidelines (KOD-211, TOYOBO). The amplified fragments were subsequently inserted into pFUSE-hIgG1Fc2 (pfc1-hg1e2, InvivoGen) to generate pFUSE-mEcrg4 (32-70)-hIgG1Fc2 and pFUSE-mEcrg4 (71-132)-hIgG1Fc2. For fragment 133-148, complementary sense and antisense oligonucleotides were annealed and inserted into pFUSE-hIgG1Fc2, yielding pFUSE-mEcrg4 (133-148)-hIgG1Fc2. Details regarding all oligonucleotide DNA primers are provided in Table S3. All constructs were verified by DNA sequencing using the BigDye Terminator Kit v3.1 (4337455, Thermo Fisher) and a 3130xl Genetic Analyzer (Thermo Fisher).

Cell culture

HEK293T cells (RCB2202, RIKEN BRC) were grown in DMEM (044-29765, FUJIFILM Wako) supplemented with 10% fetal calf serum (FCS; S1580, BioWest), 1% penicillin, and streptomy-

cin (26253-84, Nacalai Tesque). Rat primary OLG precursor cells (OPCs) were prepared and cultured as previously described [23]. OLGs were differentiated from OPCs by mitogen depletion, as previously reported [23]. Neurons were derived from ReN cells, a human neural precursor cell line (SCC008, Merck), following established protocols [24]. The MTT assay (V13154, Thermo Fisher) was used to assess cell proliferation [25].

Immunocytochemistry

Immunocytochemical staining was performed as described previously [11, 26]. HEK293Ts were transfected with expression vectors using polyethylenimine (23966-1, Polyscience), following the method described previously [27]. At 72 h post-transfection, cells were fixed with 2% paraformaldehyde in PBS (158127, Merck) for 10 min at RT, followed by incubation in blocking buffer consisting of 50% FCS and 0.3% Triton X-100 (T8787, Merck) in PBS for 30 min at RT. Cells were then incubated with primary antibodies (1 μg/ml), either 2A8 or OB1264, diluted in blocking buffer for 2 h at RT. Human, mouse, and rabbit Fc fragments were detected using Alexa Fluor 488-conjugated goat anti-human IgG (1:1000, A11013, ThermoFisher) and Alexa 594-conjugated goat anti-mouse or rabbit IgG (1:1000, A11032 or A-11012, respectively, ThermoFisher).

Cell death was evaluated using a rabbit anti-cleaved caspase 3 antibody (1:1000, #9664, Cell Signaling Technology), followed by Alexa Fluor 488-conjugated goat anti-rabbit IgG (1:1000, A11008, ThermoFisher), as described previously. Nuclei were counterstained with Hoechst 33342 (1 μg/ml, R37605, ThermoFisher), and fluorescence images were captured using an AxioImager M1 microscope (430004-9901, Zeiss).

Western blotting (WB)

WB was performed as previously described [28]. Briefly, HEK293T cells were transfected with expression vectors (pFUSE-hIgG1-Fc2, pFUSE-mEcrg4 (32-70)-hIgG1Fc2, pFUSE-mEcrg4 (71-132)-hIgG1Fc2, and pFUSE-mEcrg4 (133-148)-hIgG1Fc2) employing EndoFectin as per the manufacturer's guidelines (EF013, GeneCopoeia). At 72 h post-transfection, cell lysates were prepared in RIPA buffer, subjected to electrophoresis, and transferred onto a Hybond-P membrane (GE10600100, Amersham). The membranes were incubated with primary antibodies against Ecrg4 (1 μg/ml; OB1264 or 2A8) and GAPDH (1:1000; MAB374, Chemicon). Signals were detected using HRP-conjugated secondary antibodies, including goat anti-mouse IgG (1:5000, sc-2005, Santa Cruz Biotechnology), goat anti-rabbit IgG, and goat anti-human IgG (A120-101P and A80-118P, Bethyl Laboratories). Protein bands were visualized using an ECL system (RPN2109, Amersham), and images were acquired using a ChemiDoc MP Imaging System (12003154, Bio-Rad).

Aβ40 and Aβ42 ELISA assay

The concentrations of Aβ40 and Aβ42 in plasma and CSF were measured using Human/Rat β Amyloid 40 and 42 ELISA Kits (294-62501, 290-62601, FUJIFILM Wako), according to the supplier's protocol. Representative standard curves for Aβ40 and Aβ42 are shown in Figure S1D and S1E, respectively.

RNA sequencing analysis of plasma from dementia, MCI, and non-dementia patients

Total RNA, including miRNA, was isolated from mixed plasm samples from ECRG4-positive and -negative AD patients using the miRNeasy Plasma/Serum Kit (217004, QIAGEN). RNA samples was subsequently subjected to RNA sequencing analysis (Eurofins, Figure S3). Differential gene expression analysis was performed using iDEP to identify genes with significantly altered expression levels among the groups [30].

Quantitative reverse-transcription PCR (RT-qPCR)

Total RNA was extracted from plasma, culture supernatants, and cells using the miRNeasy kit for plasma/serum and the mirVana miRNA isolation kit (AM1560, ThermoFisher), respectively, following the manufacturers' instructions. Total RNA extracted from plasma and culture supernatants were reverse-transcribed into cDNA using the QuantiTect Reverse Transcription Kit (204143, QIAGEN), while total RNA from the cells was reverse-transcribed using the ReverTra Ace qPCR RT Kit (FSQ-201, TOYOBO). Additionally, small RNAs, including miRNAs and piRNAs, were reverse-transcribed using the miRCURY LNA Kit (339320, QIAGEN).

Real-time PCR was performed on a StepOnePlus system (4376600, Thermo Fisher) using THUNDERBIRD SYBR qPCR Mix (QPS-201, TOYOBO) for mRNA analysis and the miRCURY LNA miRNA PCR assay (339306, QIAGEN) for *let-7b* (YP00204750). The PCR conditions for mRNAs were as follows: initial denaturation at 95°C for 1 min; 40 cycles of 95°C for 15 s, and 60°C for 30 s. For *let-7b*: 95°C for 2 min; 40 cycles of 95°C for 10 s, and 56°C for 1 min. Relative RNA expression levels were calculated using the ΔΔCt method, with normalization to let-7b for plasma and culture supernatants, and to 18S rRNA for cellular samples. Primer sequences are provided in Table S3.

Preparation of brain and plasma from mice injected with ECRG4 (71-107)

ECRG4 (71-107) peptide was synthesized by GL Biochem (Shanghai) Ltd. Five microliters of either ECRG4 (71-107) solution (20 μM in 1% DMSO-PBS) or 1% DMSO-PBS alone (DMSO, D4540, Sigma) was administered into the brain parenchyma of 8-10-week-old C57BL/6 mice on alternate days, totaling five injections, as previously described [26]. Two days after the final injection, mice were euthanized, and brain tissues and blood samples were collected. Brain tissues were embedded in Tissue-Tek OCT compound (4583, Miles) and stored at -80°C, and plasma was prepared using standard procedures. Sagittal brain sections (14 μm thick) brains were prepared and immunolabeled with mouse anti-galactocerebroside (GalC) (supernatant, diluted 1:10) for OLGs [31], mouse anti-CD31 (Abcam, ab24590) for endothelial cells, and goat anti-PDGFRα (5 μg/ml, Neuromics, GT15150) for OPCs. Extravascular mouse IgG (ExV-IgG) signal was calculated by subtracting intravascular IgG signals from total IgG signal and quantified using ImageJ software (version 1.52a).

Immunohistochemistry

Immunohistochemistry was performed on paraffin-embedded human hippocampal sections (6 μm thick), as previously described [26, 28]. In brief, sections were subjected to antigen retrieval using HistoVT One (06578-55, Nacalai Tesque) according to the manufacturer's instructions, followed by permeabilization with 0.3% Triton X-100/PBS. After blocking with 2% skim milk and 0.3% Triton X-100 in PBS for 1 h, sections were incubated with primary antibodies at 4°C for 16 h. The following primary antibodies were employed: mouse anti-CD31 (ab24590, Abcam), goat anti-PDGFRα (5 μg/ml, GT15150, Neuromics), UEA-I-Biotin (0.1 μg/ml, J219, J-OIL MILLS) for human endothelial cells, mouse anti-NG2 (10 μg/ml, MAB2585, R&D), and chick anti-glial fibrillary acidic protein (GFAP) (1:200, NBP1-05198, Novus Biologicals). Signals were detected using appropriate secondary antibodies, including Alexa 488-conjugated goat anti-mouse and anti-human IgG (1:1000, A11001 and A11013, ThermoFisher), Alexa 594-conjugated goat anti-mouse, anti-rabbit, and anti-chick IgG (1:1000, A11032, A-11012 and A11042, ThermoFisher), Alexa 594-conjugated donkey anti-goat IgG (1:1000, A11058, ThermoFisher), Alexa 647-conjugated goat anti-mouse IgG (1:1000, A21235, ThermoFisher), and streptoavidine-Cy5 (0.5 μg/ml, 016-170-084, Jackson ImmunoResearch).

Statistics

Statistical analyses were conducted using GraphPad Prism and SPSS software. Data were presented as the mean ± standard deviation (SD). For comparisons between two groups, unpaired two-tailed Student's t-tests were applied, whereas one-way analysis of variance (ANOVA) followed by Tukey's post-hoc test was employed for comparisons among multiple groups, unless otherwise noted in the figure legends. Normality of the data distribution was determined by the Shapiro-Wilk test. As key variables (ECRG4, Aβ40, Aβ42, and the Aβ42/Aβ40 ratio) did not follow a normal distribution, Spearman's rank correlation analysis was applied to evaluate their associations. To investigate whether plasma ECRG4 independently predicts AD, binary logistic regression analysis was performed using the enter method, with adjustment for Aβ40, Aβ42, Aβ42/Aβ40 ratio, age, and sex. Results were reported as odds ratios (OR) with 95% confidence intervals (CI). Diagnostic accuracy was assessed using receiver operating characteristic (ROC) curve analysis, and the area under the curve (AUC) was calculated. A combined model incorporating ECRG4, the Aβ42/Aβ40 ratio, and age was utilized to assess the incremental predictive value of ECRG4.

Table 1. Percent of ECRG4-positive patients with dementia, mild cognitive impairment (MCI) and non-dementia with neurological disorders

Diagnosis		Total	Male	Female
Dementia	Alzheimer's disease (AD)	47.3% (61/129)	44.4% (24/54)	49.3% (37/75)
	Non-AD	60% (18/30)	64.3% (9/14)	56.3% (9/16)
MCI		25% (7/28)	9.1% (1/11)	35.3% (6/17)
Non-dementia		5% (4/80)	10% (4/40)	0% (0/40)

Results

Establishment of a novel sandwich ELISA for quantifying human ECRG4

To establish a novel sandwich ELISA for quantifying ECRG4, we developed four distinct mouse anti-ECRG4 antibodies (3B4, 2A8, 1H4, and 1A3), each targeting specific regions of the ECRG4 protein (Figure S1A). Various combinations of these mouse Abs with a rabbit anti-ECRG4 Ab (OB1264) were evaluated to identify the optimal antibody pair for detecting ECRG4 (71-148), corresponding to the AUGURIN precursor.

As illustrated in Figure S1B, ECRG4 (71-148) was detected in a dose-dependent manner when OB1264 served as the detection antibody in combination with either 1H4 or 2A8 as the capture antibody. In contrast, no signal was observed when OB1264 was paired with either 3B4 or 1A3. Notably, the combination of OB1264 and 2A8 produced a stronger signal than that of OB1264 and 1H4, and was therefore selected for subsequent ELISA development. Furthermore, we observed that the combination of 2A8 and OB1264 (both at 1 μg/ml) demonstrated higher sensitivity in detecting ECRG4 (71-132) peptide compared with ECRG4 (71-148) (Figure S1C). Consequently, ECRG4 (71-132) was selected as the positive control for the assay.

To verify the specificity of these Abs, WB and immunocytochemical analyses were performed using HEK293T cells expressing ECRG4 fragments (32-70, 71-132, and 133-148), each fused with human IgG (hIgG). As shown in Figure S2A, both OB1264 and 2A8 successfully detected the ECRG4 (71-132)-hIgG fusion protein, with no detectable reactivity in the other fusion constructs. Consistently, immunocytochemical analysis demonstrated that both antibodies specifically labeled cells overexpressing ECRG4 (71-132)-hIgG, without detectable staining in cells expressing other constructs (Figure S2B, S2C). These results indicate that a novel ELISA for ECRG4 quantification was successfully established using 2A8 as the capture antibody and OB1264 as the detection antibody, utilizing the combination of OB1264 and 2A8.

Elevated plasma ECRG4 levels in patients with MCI and AD

Plasma ECRG4 concentrations in individuals with dementia (including both AD and non-AD types, as specified in Table S1), MCI, and non-dementia neurological disorders (Table S2) was quantified using the established ELISA. ECRG4 was detectable across all diagnostic categories. Among dementia patients, 50% (79/159) were ECRG4-positive, compared with 25% (7/28) in the MCI group and 5% (4/80) in the non-dementia group (**Table 1**). Within the dementia cohort, ECRG4-positivity was observed in 49% (33/68) of males and 51% (46/91) of females. Among MCI patients, the positivity rates were 9% (1/11) in males and 35% (6/17) in females. Stratified by diagnosis, 47% (61/129) of AD patients and 60% (18/30) of non-AD dementia patients were ECRG4-positive. Within the AD group, ECRG4 detection rates were 44% (24/54) in males and 49% (37/75) in females.

Furthermore, we observed a correlation between ECRG4 positivity and disease severity reflected by MMSE score [29-31]. Patients with MMSE scores < 23 exhibited a higher ECRG4 positivity rate (34%) compared with individuals with MCI (MMSE 24-27), in whom the positivity rate was 13% (**Table 2**). These findings suggest that plasma ECRG4 may reflect disease severity.

Mean plasma ECRG4 levels were 0.85 ng/ml in MCI (males: 0.45, females: 1.18), 1.00 ng/

Table 2. Mini Mental State Examination (MMSE) distribution of the dementia and MCI patients with increased plasma-ECRG4

Cognitive functioning tests	Total	Male	Female
MMSE ≤ 23	34.3% (23/67)	32.1% (11/21)	38.9% (12/46)
MMSE 24-27	12.9% (4/31)	16.7% (2/12)	10.5% (2/19)
MMSE ≥ 28	22.2% (4/18)	10.0% (1/10)	37.5% (3/8)

ml in AD (males: 1.02, females: 0.99), 0.37 ng/ml in non-AD dementia (males: 0.44, females: 0.31), and 0.08 ng/ml in non-dementia patients (males: 0.15, females: 0) (**Figure 1A**, **1B**). Notably, ECRG4 was undetectable in the plasma of healthy controls (data not shown). Increased Aβ formation in the brain parenchyma is known to reduce Aβ40 and Aβ42 levels in the plasma and CSF of patients with AD [32, 33]. In plasma, the mean plasma Aβ40 levels were 82 pmol in MCI patients (males: 90 pmol, females: 77 pmol), 85 pmol in AD (males: 87 pmol, females: 84 pmol), and 71 pmol in non-AD dementia (males: 69 pmol, females: 74 pmol), compared with 105 pmol in non-dementia controls (males: 99 pmol, females: 111 pmol). Similarly, mean plasma Aβ42 levels were 10.5 pmol in MCI (males: 12.8 pmol, females: 9.1 pmol), 9.7 pmol in AD (males: 9.6 pmol, females: 9.8 pmol), and 7.2 pmol in non-AD dementia (males: 6.9 pmol, females: 7.4 pmol), compared with 11.5 pmol in non-dementia individuals (males: 10.4 pmol, females: 12.6 pmol) (**Figure 1C-F**). These findings indicate a consistent reduction of both Aβ40 and Aβ42 levels in dementia and MCI groups relative to non-dementia controls. Although the Aβ42/Aβ40 ratio is generally expected to decrease in patients due to preferential aggregation of Aβ42 [32, 33], there were no significant differences in the plasma Aβ42/Aβ40 ratio among the groups (**Figure 1G**, **1H**).

In CSF, both Aβ40 and Aβ42 levels were lower in MCI, AD, and non-AD patients compared with non-dementia controls. Specifically, the mean CSF Aβ40 levels were 900 pmol for MCI group (males: 923 pmol, females: 885 pmol), 909 pmol for AD group (males: 899 pmol, females: 916 pmol), 1,029 pmol for non-AD group (males: 1,021 pmol, females: 1,037 pmol), and 1,154 pmol for non-dementia group (males: 1,245 pmol, females: 1,063 pmol); and the mean Aβ42 levels were 104 pmol for MCI (males: 120 pmol, females: 94 pmol), 107 pmol for AD (males: 109 pmol, females: 106 pmol), 129 pmol for non-AD (males: 137 pmol, females: 121 pmol), and 152 pmol for non-dementia (males: 171 pmol, females: 134 pmol) (**Figure 2A-D**). However, the CSF Aβ42/Aβ40 ratio did not differ significantly among groups (**Figure 2E**, **2F**). Additionally, ECRG4 levels in CSF remained stable across diagnostic categories (**Figure 2G**, **2H**).

Spearman correlation analyses revealed that plasma ECRG4 levels were significantly negatively correlated with Aβ40 (ρ = -0.437, $P < 0.001$), Aβ42 (ρ = -0.455, $P < 0.001$), and the Aβ42/Aβ40 ratio (ρ = -0.305, $P < 0.001$) (Table S4; **Figure 3A-C**). Conversely, strong positive correlations were observed between Aβ40 and Aβ42, as well as between these biomarkers and the Aβ42/Aβ40 ratio (ρ = 0.703, $P < 0.001$; ρ = 0.150, P = 0.014) (Table S4). No significant correlation was detected between CSF ECRG4 levels and amyloid biomarkers (Aβ40, Aβ42, or Aβ42/Aβ40 ratio) (Table S5).

To evaluate the predictive value of plasma ECRG4, multivariate logistic regression analysis was performed. ECRG4 (P = 0.001, OR = 2.253), Aβ40 (P = 0.001, OR = 0.925), Aβ42 (P = 0.001, OR = 2.040), Aβ42/Aβ40 ratio (P = 0.007, OR < 0.001), and age ($P < 0.001$, OR = 1.091) were identified as independent predictors of AD (**Figure 3D**, **3E**).

ROC curve analysis further demonstrated that plasma ECRG4 alone yielded an area under the curve (AUC) of 0.62 (95% CI: 0.5569), indicating moderate discriminatory capability (**Figure 4A**). However, traditional amyloid biomarkers (Aβ40, Aβ42, and their ratio) in CFS samples demonstrated higher discriminatory capability compared with ECRG4 (**Figure 4B**). Importantly, integrating ECRG4 with the Aβ42/Aβ40 ratio increased the AUC to 0.70, and the further inclusion of age in this multivariate model elevated the AUC to 0.80 (**Figure 4C**), demonstrating enhanced diagnostic performance.

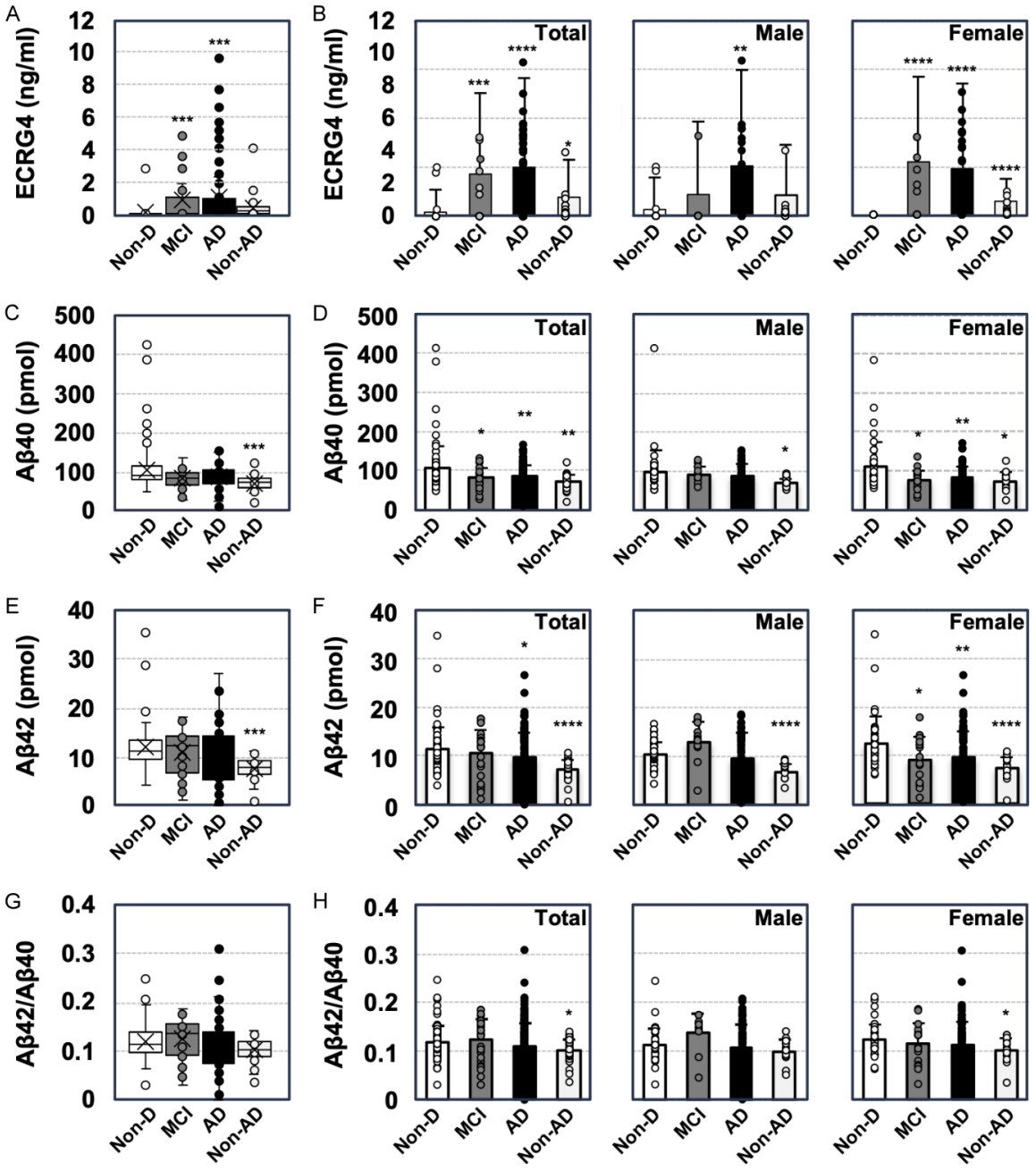

Figure 1. Esophageal cancer related gene 4 (ECRG4), Amyloid beta (Aβ)40, and Aβ42 concentrations in the plasma of dementia, mild cognitive impairment (MCI), and non-dementia patients. (A) ECRG4 concentrations in the plasma of patients categorized as non-dementia (non-D, white column), MCI (dark gray column), AD (black column), and non-AD (light gray column). (B) Sex-disaggregated quantitative data corresponding to (A). (C) Aβ40 concentration in the plasma of individuals classified as non-D, MCI, AD, and non-AD. (D) Sex-disaggregated quantitative data corresponding to (C). (E) Aβ42 concentration in the plasma of individuals classified as non-D, MCI, AD, and non-AD. (F) Sex-disaggregated quantitative data corresponding to (E). (G) Aβ42/Aβ40 ratio in the plasma of individuals classified as non-D, MCI, AD, and non-AD. (H) Sex-disaggregated quantitative data corresponding to (G). A one-way ANOVA was used to compare plasma ECRG4, Aβ40, Aβ42 concentrations, and the Aβ42/Aβ40 ratio among the non-dementia group, MCI group, AD group, and non-AD group. Before performing Analysis of Variance (ANOVA), we verified the normality of the data using the Shapiro-Wilk test and confirmed the homogeneity of variance among the groups using the Levene test. Subsequently, Dunnett's test was used for post hoc multiple comparisons, with the non-dementia group as a common reference group. All error bars represent the standard deviation (SD). *P* values are indicated for data showing significant differences from the non-D group. **P* < 0.05, ***P* < 0.01, ****P* < 0.001, *****P* < 0.0001.

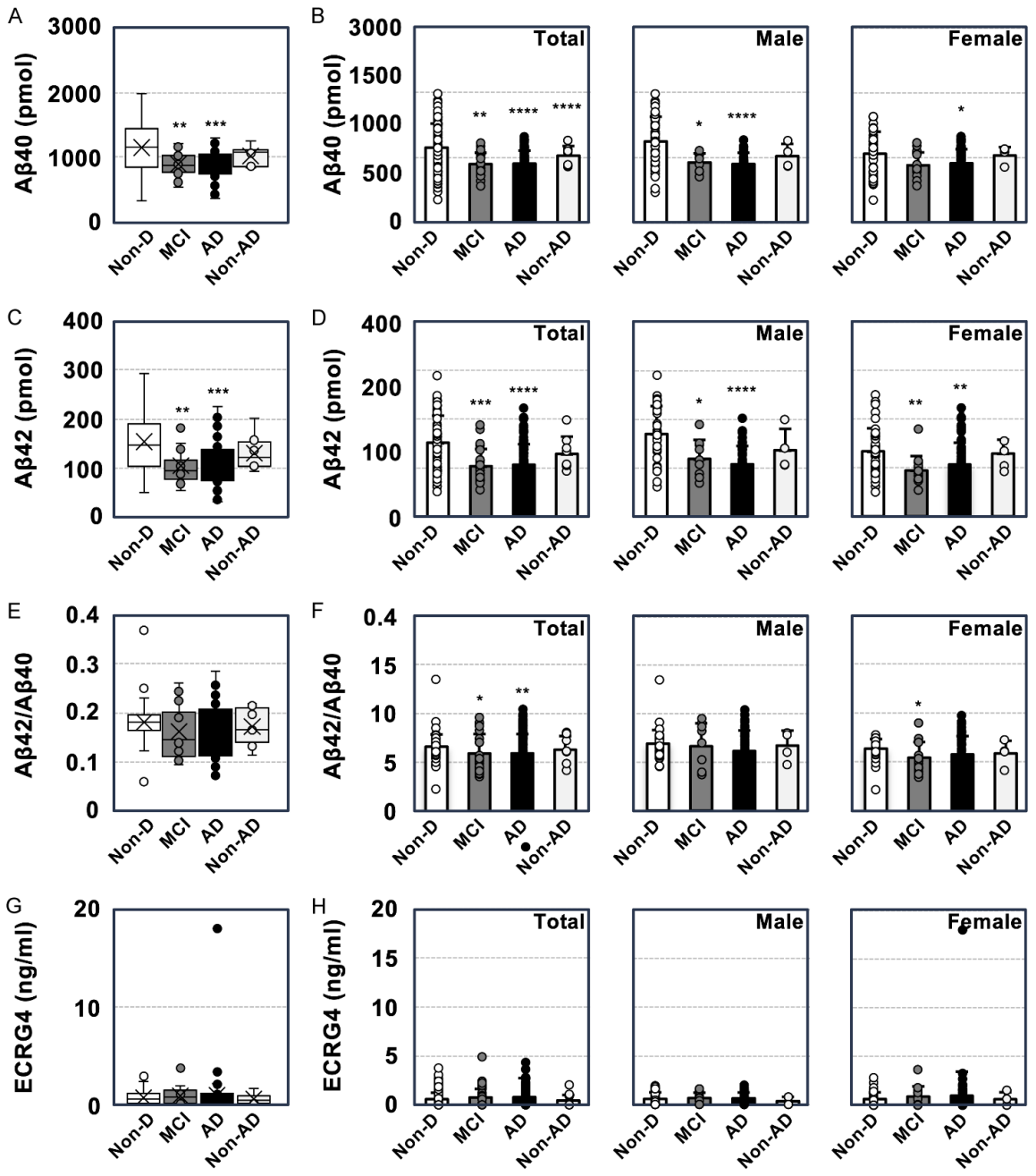

Figure 2. Concentration of ECRG4, Aβ40 and Aβ42 in Cerebrospinal fluid (CSF) of dementia, MCI and Non-dementia patients. (A) Aβ40 concentration in the CSF of patients with Non-D, MCI, AD and Non-AD. (B) Sex-disaggregated quantitative data from (A). (C) Aβ42 concentration in the CSF of patients with Non-D, MCI, AD and Non-AD. (D) Sex-disaggregated quantitative data from (C). (E) Aβ42/Aβ40 ratio in CSF of patients with Non-D, MCI, AD and Non-AD. (F) Sex-disaggregated quantitative data from (E). (G) ECRG4 concentration in CSF of patients with Non-D, MCI, AD and Non-AD. (H) Sex-disaggregated quantitative data from (G). Error bar: ± SD. A one-way ANOVA was used to compare plasma ECRG4, Aβ40, Aβ42 concentrations, and the Aβ42/Aβ40 ratio among the non-dementia group, MCI group, AD group, and non-AD group. Before performing ANOVA, we verified the normality of the data using the Shapiro-Wilk test and confirmed the homogeneity of variance among the groups using the Levene test. Subsequently, Dunnett's test was used for post hoc multiple comparisons, with the non-dementia group as a common reference group. Error bars represent ± SD. *P* values are indicated for data showing significant differences from the non-D group. **P* < 0.05, ***P* < 0.01, ****P* < 0.001, *****P* < 0.0001.

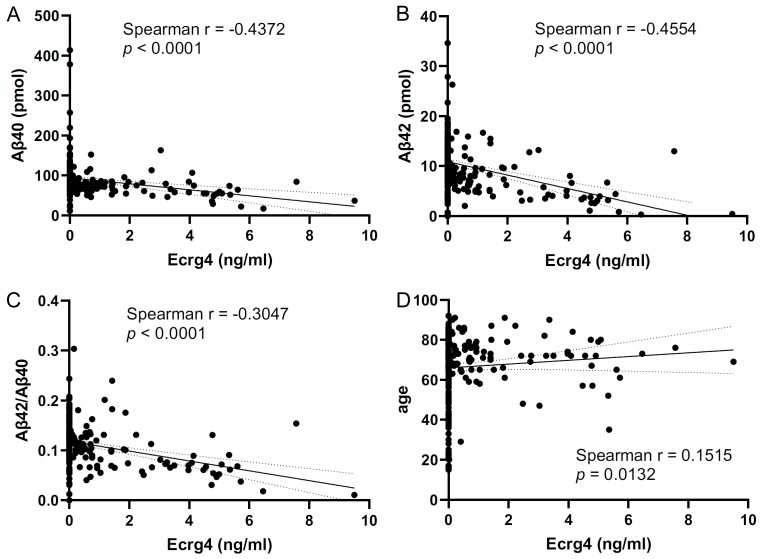

E

Variables	OR(95%CI)	P
sex	0.874(0.468~1.633)	0.673
Ecrg4	2.253(1.418~3.582)	0.001
Aβ40	0.925(0.884~0.968)	0.001
Aβ42	2.040(1.329~3.131)	0.001
Aβ42/Aβ40	< 0.001(0.000~0.000)	0.007
age	1.091(1.062~1.121)	< 0.001

Figure 3. Association between plasma ECRG4 levels and AD biomarkers and disease status. Scatter plots illustrating the Spearman correlation of plasma ECRG4 levels with (A) Aβ40, (B) Aβ42, (C) Aβ42/Aβ40 ratio, and (D) age (years). Each panel displays Spearman's *r* and the corresponding *p*-values. (E) Table presenting the odds ratios (ORs) and 95% confidence intervals (CIs) for each variable included in the multivariate logistic regression model, comparing the MCI and AD groups with the non-dementia and non-AD control groups. The model was adjusted for all variables.

In summary, plasma ECRG4 levels are elevated in patients with MCI and AD, are inversely associated with amyloid biomarkers, and provide incremental diagnostic value when combined with established markers. Therefore, ECRG4 may serve as a promising peripheral biomarker for early detection and risk stratification of MCI and AD.

ECRG4 (71-107) diminished extracellular CHST3 mRNA by inducing apoptosis in oligodendrocytes

Given that ECRG4 was detectable in approximately half of AD patients, we conducted a comparative analysis between ECRG4-positive and ECRG4-negative individuals. RNA sequencing of plasma samples identified several RNAs that were differentially expressed between the two groups (Figure S3). Our research focused on circulating mRNAs, as they facilitate functional interpretation and inference of their cellular origins compared with other RNA types. Using iDEP analysis, three genes - solute carrier family 46 member 3 (SLC46A3), carbohydrate sulfotransferase (CHST3), and tetratricopeptide repeat domain 39A (TTC39A) - were identified as significantly downregulated in ECRG4-positive patients compared to ECRG4-negative patients (**Figures 5A**, S4). These expression patterns were validated using RT-qPCR (**Figure 5B**).

According to the Human Protein Atlas (HPA), SLC46A3 and TTC39A are predominantly expressed in neurons, whereas CHST3 is expressed in both OLGs and OPCs [34]. This observation aligns with previous reports indicating that both neurons, particularly GABAergic neurons, and OLGs are compromised in the brains of AD patients [35].

To assess the impact of ECRG4 on neural cell populations, neurons and OLG lineage cells were cultured in the presence of various ECRG4-derived peptides, and cell viability was assessed using the MTT assay. While none of the peptides affected neuronal survival, ECRG4 (71-107) induced cell death in OLG lineage cells (**Figure 5C**). To further evaluate the cytotoxicity of ECRG4 (71-107) in these cells, OLGs and OPCs were cultured separately with ECRG4 (71-107), followed by immunostaining for cleaved caspase 3 (Casp3), an apoptosis marker. Our results showed that ECRG4 (71-107) selectively induced apoptosis in OLGs but not in OPCs (**Figure 5D**, **5E**).

Subsequently, we examined whether ECRG4 (71-107) affected Chst3 mRNA levels. OPCs and OLGs were cultured separately in the presence of DMSO or peptides, and Chst3 mRNA levels were measured in both cell lysates (**Figure 5F**) and culture supernatant (**Figure 5G**) using RT-qPCR. Our findings demonstrated that

A

Test Result Variable(s)	Area (AUC)	Std. Error	Asymptotic Significance (Sig.)	95% Confidence Interval
ECRG4	0.6187	0.03407	0.0008	0.5520 to 0.6855
Aβ40	0.5095	0.03587	0.7896	0.4392 to 0.5798
Aβ42	0.5500	0.03545	0.1602	0.4805 to 0.6195
Aβ42/Aβ40	0.5508	0.03545	0.1534	0.4813 to 0.6203

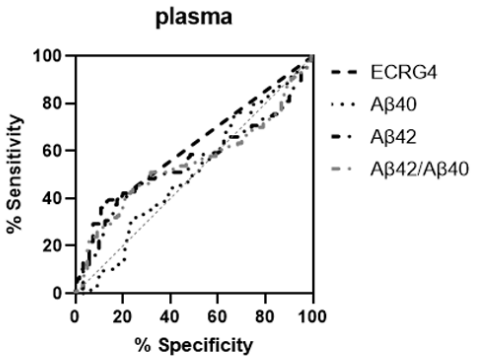

B

Test Result Variable(s)	Area (AUC)	Std. Error	Asymptotic Significance (Sig.)	95% Confidence Interval
ECRG4	0.5414	0.04162	0.3153	0.4598 to 0.6230
Aβ40	0.7043	0.03948	< 0.0001	0.6270 to 0.7817
Aβ42	0.7379	0.03509	< 0.0001	0.6692 to 0.8067
Aβ42/Aβ40	0.6059	0.04151	0.0102	0.5246 to 0.6873

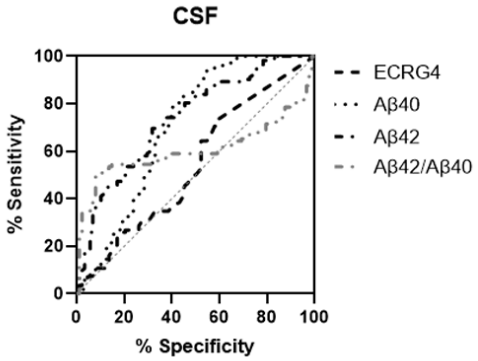

C

Test Result Variable(s)	Area (AUC)	Std. Error	Asymptotic Significance (Sig.)	95% Confidence Interval
ECRG4	0.6187	0.03407	0.0008	0.5520 to 0.6855
ECRG4+Aβ 42/Aβ40	0.6963	0.03237	< 0.0001	0.6328 to 0.7597
ECRG4+age	0.7815	0.02846	< 0.0001	0.7257 to 0.8373
ECRG4+Aβ 42/Aβ40+age	0.8009	0.02716	< 0.0001	0.7476 to 0.8541

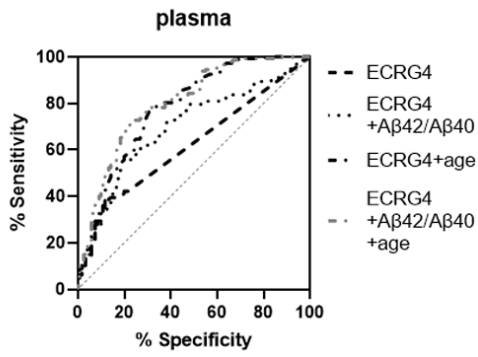

Figure 4. The integration of plasma ECRG4 with amyloid biomarkers significantly enhances diagnostic accuracy. Receiver operating characteristic (ROC) curves were developed to evaluate and compare the diagnostic performance of plasma ECRG4, Aβ42/Aβ40 ratio, and their combination in distinguishing patients with AD from non-dementia controls. A. ROC curves for individual markers in plasma samples. B. ROC curves for individual markers in CSF samples. C. ROC curves for combination models in plasma, incorporating ECRG4 with Aβ42/Aβ40 ratio, and age. The area under the curve (AUC) values are shown in the plot.

ECRG4 (71-107) significantly reduced Chst3 mRNA levels in OLGs but not in OPCs. Similarly, ECRG4 (71-107) decreased Chst3 mRNA levels in the supernatant of OLGs, but not in the supernatant of OPCs. Although both OPCs and OLGs express Chst3 mRNA, the levels detected in the OPC culture supernatants were markedly lower than those in the OLG cultures, suggesting that OLGs are the primary source of circulating CHST3 mRNA. These findings collectively suggest that ECRG4 (71-107) induces apoptosis in OLGs, contributing to a reduction in extracellular CHST3 mRNA levels. This decrease may reflect OLG injury and could serve as a passive biomarker associated with AD pathology.

Intracranial administration of ECRG4 (71-107) reduced plasma Chst3 levels and induced blood-brain barrier (BBB) disruption

We subsequently explored the effects of ECRG4 (71-107)-induced OLG cytotoxicity on plasma

A

Patients plasma	RNA-UMIs			
	SLC46A3	*CHST3*	*TTC39A*	*let7b*
ECRG4 positive	0	0	11	14,712
ECRG4 negative	265	554	281	13,267

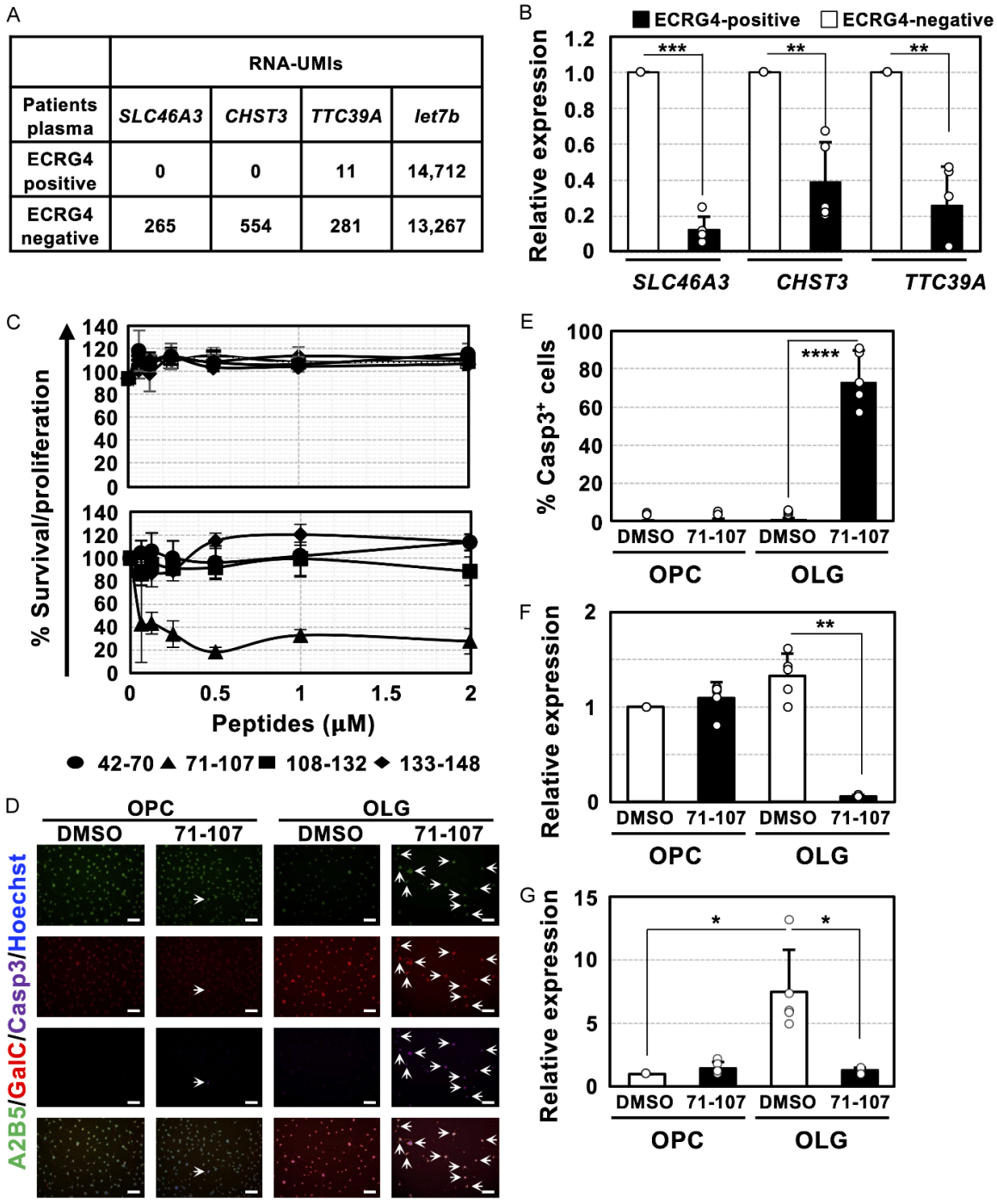

Figure 5. Cytotoxicity of ECRG4 (71-107) toward oligodendrocytes. (A) Expression levels of three candidate genes, Solute carrier family 46 member 3 (SLC46A3), Carbohydrate sulfotransferase 3 (CHST3), and Tetratricopeptide repeat domain 39A (TTC39A), along with the control microRNA let-7b, were analyzed in ECRG4-positive and -negative plasma using RNA-seq. UMIs: Unique Molecular Identifiers. (B) Expression of SLC46A3, CHST3, and TTC39A in ECRG4-positive (black) and -negative (white) plasma was measured by RT-qPCR. (C) The proportion of proliferating/surviving neurons (upper figure) and oligodendrocyte lineage cells (lower figure) was assessed in cultures treated with ECRG4 peptides: 42-70 (circle), 71-107 (triangle), 108-132 (square), and 133-148 (diamond). (D) Nuclei were counterstained with Hoechst 33342 (blue). Immunofluorescence images of oligodendrocyte precursor cells (OPCs) and oligodendrocytes (OLGs) treated with Dimethyl sulfoxide (DMSO) or peptide 71-107, showing A2B5 (green), Galactocerebroside (GalC) (red), and Cleaved Caspase 3 (Casp3) (purple). Arrows denote Casp3-positive cells. Scale bar: 100 μm. (E) The percentages of cleaved Casp3-positive cells, OPCs, and OLGs were assessed in cultures

treated with DMSO (white columns) or peptide 71-107 (black columns). (F) Relative expression of Chst3 was measured in OPC and OLG cells cultured with either DMSO alone (white column) or peptide 71-107 (black column). (G) Relative Chst3 mRNA levels were quantified in the supernatant of OPC and OLG cells cultured with DMSO (white column) or peptide 71-107 (black column). Error bars represent ± SD. Statistical significance was determined as follows: (B, E-G) for two-group comparisons, unpaired two-tailed t-tests were used. *$P < 0.05$, **$P < 0.01$, ***$P < 0.001$, ****$P < 0.0001$.

levels of ECRG4 (108-132) peptide fragment in AD patients. Seo et al. reported that OPCs respond to white matter injury and contribute to BBB disruption [36]. Similarly, Niu et al. found that OPCs in multiple sclerosis model mice aggregate around perivascular regions, increasing vascular permeability by compromising the BBB through a Wnt inhibitory factor 1 (Wif1)-dependent mechanism [37]. Based on these findings, we hypothesized that OPC activation and perivascular clustering following ECRG4 (71-107)-induced OLG damage may compromise BBB integrity.

To test this hypothesis, we introduced the peptide into the brain parenchyma of mice (**Figure 6A**). Immunofluorescence analysis was performed using markers for OLGs (GalC), endothelial cells (CD31), OPC (PDGFRα), and endogenous mouse IgG to assess BBB integrity. As shown in **Figure 6B** and **6C**, peptide injection led to a significant reduction in GalC signal intensity by approximately 47%, indicating OLG loss or damage. Additionally, plasma Chst3 mRNA levels were reduced by approximately 32% in peptide-treated mice (**Figure 6D**), consistent with findings in AD patients (**Figure 5A**, **5B**).

Immunostaining revealed a notable increase in extravascular IgG (ExV-IgG) signals in peptide-injected brains, indicating peptide-dependent BBB disruption (**Figure 6E-G**). In parallel, a marked increase in PDGFRα$^+$ OPCs was observed, with these cells clustering around blood vessels (BVs) (**Figure 6H-J**). Moreover, the extent of OPC clustering positively correlated with ExV-IgG signal intensity (**Figure 6K**). Collectively, in AD patients, ECRG4 (71-107)-induced OLG cytotoxicity, accompanied by reduced plasma Chst3 levels and BBB impairment, potentially associated with OPC activation and perivascular clustering.

Increased OPC number and perivascular clustering in EAD

To investigate OPC dynamic in human AD, immunohistochemical analyses were performed on hippocampal sections from individuals with EAD, AD, and non-dementia controls, all possessing the APOE 3/3 genotype. OPCs, astrocytes, and endothelial cells were labeled using NG2, GFAP, and UEA1, respectively. Our findings showed an increase in both OPC number and OPC clusters - defined as aggregates of more than three cells - around BVs in EAD samples, similar to observations in the brains of ECRG4 (71-107)-injected mice (**Figure 7A-C**). In contrast, OPC numbers in AD patients were comparable to those in non-demented controls. These findings suggest that OPC accumulation and clustering around BVs are significantly altered during AD progression. Furthermore, a reduction in GFAP$^+$ astrocytes was observed in patients with AD (**Figure 7D**), indicating that astrocytic impairment at later stages of AD. This evidence supports the notion that OPC clustering-induced BBB breakdown facilitates ECRG4 peptide entry into the circulation in early AD.

Discussion

In the present study, we identified a significant elevation of ECRG4 in the hippocampus of patients with EAD and AD (Lai Kit et al, unpublished observation), and subsequently developed a highly sensitive ELISA for ECRG4 detection. This assay successfully detected ECRG4, particularly peptides containing the 108-132 region, in the plasma of approximately 25% of patients with MCI and 50% of those with AD. Notably, plasma ECRG4 levels were negatively correlated with Aβ biomarkers. Furthermore, integration of ECRG4 with the Aβ42/Aβ40 ratio and age significantly enhanced diagnostic accuracy (AUC = 0.80) for distinguishing MCI and AD. Mechanistically, intracerebral injection of ECRG4 (71-107) in mice resulted in OLG cytotoxicity and BBB disruption, which are associated with OPC clustering around BVs. Similar pattern was observed in the hippocampus of EAD patients. Collectively, these findings suggest that elevated ECRG4 levels in the bloodstream may reflect, or be associated with, OLG injury and BBB dysfunction during EAD.

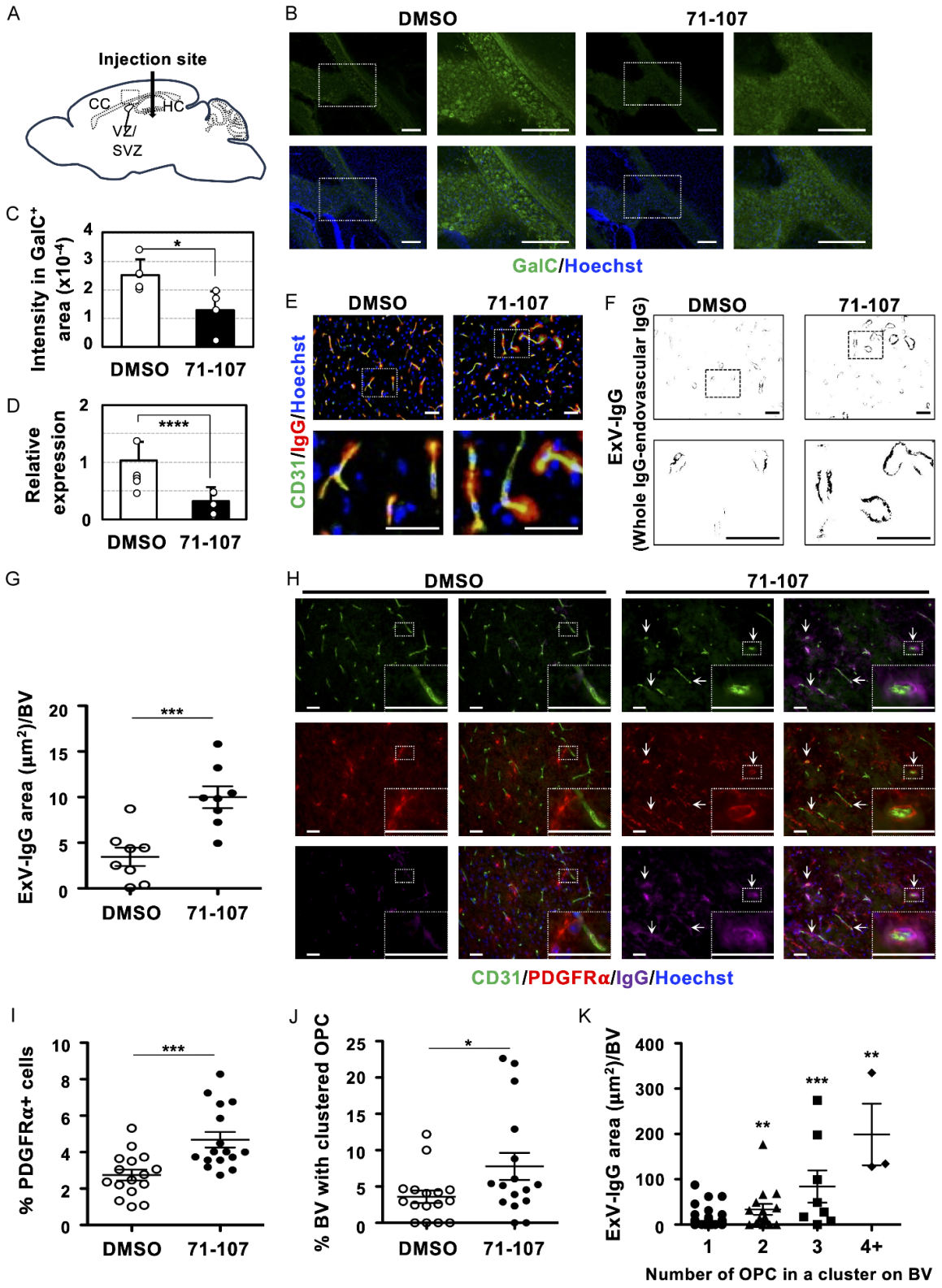

Figure 6. Intracranial injection of ECRG4 (71-107) decreases galactocerebroside levels and induced Blood Brain Barrier (BBB) leakage with OPC clustering on blood vessels. (A) Schematic representation of the ECRG4 (71-107) injection site. (B) Representative images depicting immunoreactivity for GalC (green) in brains injected with either DMSO alone (left panels) or ECRG4 (71-107) (right panel). (C) Quantitative analysis of GalC$^+$ area intensity in the

corpus callosum injected with either DMSO alone (white column) or ECRG4 (71-107) (black column). (D) Relative expression levels of Chst3 mRNA in the plasma of mice injected with either DMSO alone (white column) or ECRG4 (71-107) (black column). (E) Representative images illustrating immunoreactivity for the endothelial marker CD31 (green) and mouse immunoglobulin G (mIgG) (red) in mouse brains injected with either DMSO alone (left panels) or ECRG4 (71-107) (right panels). The lower panels show high-magnification images of the boxed area outlined by the white dotted line in the upper panels. (F) Representative images of extravascular mouse IgG (ExV-IgG) generated by removing endovascular IgG from whole IgG. (G) Quantitative data of ExV-IgG area per BV. (H) Representative images showing immunoreactivity for CD31 (green), the OPC marker platelet-derived growth factor receptor α (PDGFRα) (red), and IgG (purple) in brains injected with either DMSO alone (left panels) or ECRG4 (71-107) (right panels). Arrows indicate the OPC clusters in the blood vessel (BV). (I) Percentage of PDGFRα$^+$ cells, as shown in (H). (J) Percentage of BV with clustered OPC, as shown in (H). (K) Quantitative data of ExV-IgG area per number of OPC in a cluster on BV. All nuclei were counterstained with Hoechst 33342 (blue). Error bars represent ± SD. Statistical comparisons between the DMSO control and ECRG4 (71-107) treatment groups were performed using unpaired two-tailed t-tests for each independent experimental endpoint (C, D, G, I, J, and K). As each comparison tested a distinct, pre-planned hypothesis, no adjustment for multiple comparisons was applied. *P < 0.05, **P < 0.01, ***P < 0.001, ****P < 0.0001. Scale: 100 μm.

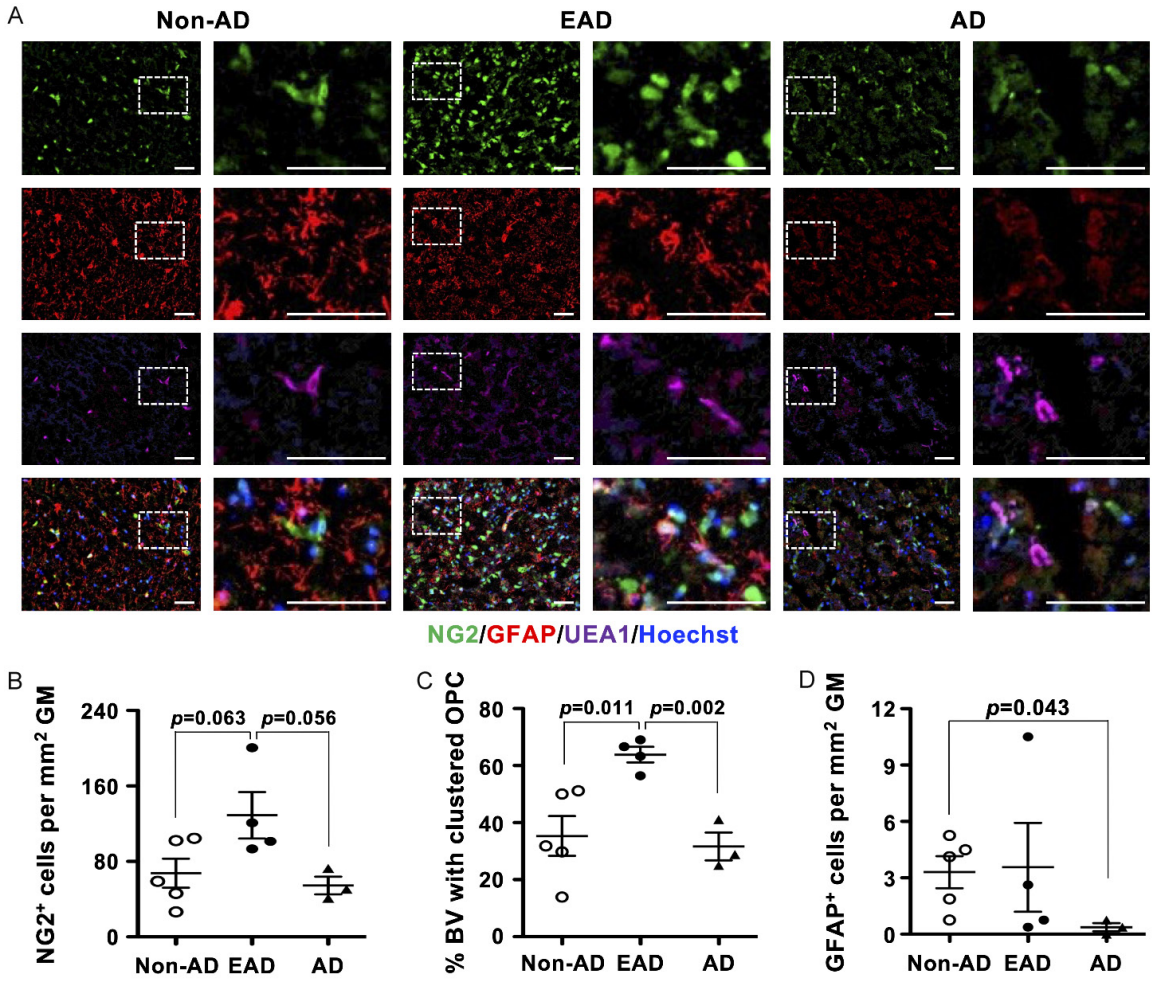

Figure 7. OPCs transiently increased and formed clusters on BV in the hippocampus during EAD. A. Representative images depicting immunoreactivity for the OPC marker Neural-glial antigen 2 (NG2) (green), astrocyte marker glial fibrilary acidic protein (GFAP) (red), and endothelial-specific Ulex Europaeus Agglutinin 1 (UEA1) signal (purple) within the hippocampus of non-AD individuals (left panels), EAD individuals (middle panels), and AD individuals (right panels). The right panels for each sample show high-magnification images of the boxed area delineated by a white dotted line in the left panel. All nuclei were counterstained with Hoechst 33342 (blue). Scale: 100 μm. B. Quantification of NG2-positive cells per square millimeter in the gray matter of non-AD, EAD, and AD patients. C. Percentage of BV with clustered OPCs. D. Quantification of GFAP-positive cells per square millimeter in the gray matter of non-AD, EAD, and AD patients. Error bars represent ± SD. Statistical significance was assessed using one-way ANOVA, followed by Tukey's test.

Despite these findings, the cellular origin of ECRG4 in the brain remains unclear. Data from HPA indicate that ECRG4 is highly expressed in the choroid plexus (https://www.proteinatlas.org/ENSG00000119147-ECRG4/brain). Consistent with this, Gonzalez et al. reported that ECRG4 cleavage in the choroid plexus is modulated by brain physiological status [38]. Accumulating evidence links choroid plexus functional defects to the development of AD [39]. Therefore, inhibiting ECRG4 production in the choroid plexus may represent a potential therapeutic strategy.

Previous studies have demonstrated that distinct ECRG4 peptides exhibit receptor-specific activities. The 71-132 fragment binds to oxidized low-density lipoprotein receptor 1 (LOX-1), whereas the 133-148 binds to toll-like receptor 4 (TLR4), each independently inducing proinflammatory factors such as IL-6 and TNFα via activation of the NF-κB signaling pathway in microglia [14, 15], thereby accelerating AD pathogenesis. In contrast, ECRG4 (71-107), which did not bind to either receptor, exerted cytotoxic effects on OLGs in our study. Further studies are needed to clarify how individual ECRG4 fragments promote AD development. Accumulating evidence suggests that OLG function and myelin impairment represent early events in AD development. Depp et al. demonstrated that myelin dysfunction drives Aβ deposition by inducing axonal swelling in AD models [40]. Similarly, Blanchard et al. showed that APOE4, a major genetic risk factor for AD, disrupts cholesterol metabolism and impairs oligodendrocyte-mediated myelination, thereby contributing to neuronal dysfunction [41]. In conjunction with our findings, these studies suggest that preventing OLG damage may lead to novel therapeutic approaches for AD.

Our study does not provide direct evidence linking the sequential events observed, namely ECRG4 (71-107)-induced OLG death, compensatory perivascular aggregation of OPCs, BBB disruption, and increased plasma levels of the ECRG4 (108-132) fragment, particularly in human samples. Therefore, future studies are required to clarify our hypothesis using targeted approaches, such as peptide neutralization, rescue of OLG viability, inhibition of OPC accumulation.

This study has several limitations. First, the sample size, particularly for MCI, non-AD dementia, and healthy control groups, was relatively small and unevenly distributed across groups, which may limit statistical power and generalizability. Validation in larger, multicenter cohorts are warranted. Second, the use of patients with other neurological disorders as control subjects may introduce confounding factors, as these conditions could involve subtle BBB alterations or neuroinflammatory processes. Third, there is no direct evidence demonstrating that plasma levels of the ECRG4 (108-132) fragment reflect the toxic effects of the ECRG4 (71-107) fragment in the brain. Finally, although our mechanistic findings provide insights into potential ECRG4-related pathways, they are preliminary and should be considered hypothesis-generating. As all experiments were conducted at a single institution using in-house reagents, further studies are needed to ensure reproducibility and consistency across different laboratories.

Future research should focus on determining whether alterations in plasma ECRG4 are specific to AD or indicative of a broader response to CNS injuries, such as cerebrovascular lesions or demyelinating disorders. These conditions may involve OLG damage or dysfunction of choroid plexus, which is known for its high expression of ECRG4.

Acknowledgements

We thank Dr. Kenju Miura for his initial support of this work and Dr. Toshihiro Hata for the immunohistochemical analysis of hippocampal sections of patients. This research was partially funded by a collaborative research grant awarded by ASUBIO Pharma Corporation (to T.K.), the Joint Research Program of the Institute for Genetic Medicine, Hokkaido University (to T.K.), JSPS KAKENHI (JP22H04923 (CoBiA) to S.M.), AMED (JP21wm0425019 to S.M.), and JST SPRING (JPMJSP2119, to L.Z.). PaperPal was used for assistance with English language editing and phrasing during the preparation of this manuscript.

Disclosure of conflict of interest

None.

Address correspondence to: Dr. Toru Kondo, Division Vision of Stem Cell Biology, Institute for Genetic Medicine, Hokkaido University, Sapporo, Hokkaido 060-0815, Japan. E-mail: tkondo@igm.hokudai.ac.jp

References

[1] Bertram L, Lill CM and Tanzi RE. The genetics of Alzheimer disease: back to the future. Neuron 2010; 68: 270-281.

[2] Querfurth HW and LaFerla FM. Mechanisms of disease Alzheimer's disease. N Engl J Med 2010; 362: 329-344.

[3] Zlokovic BV. Neurovascular pathways to neurodegeneration in Alzheimer's disease and other disorders. Nat Rev Neurosci 2011; 12: 723-738.

[4] Jack CR Jr and Holtzman DM. Biomarker modeling of Alzheimer's disease. Neuron 2013; 80: 1347-1358.

[5] Logovinsky V, Satlin A, Lai R, Swanson C, Kaplow J, Osswald G, Basun H and Lannfelt L. Safety and tolerability of BAN2401--a clinical study in Alzheimer's disease with a protofibril selective Abeta antibody. Alzheimers Res Ther 2016; 8: 14.

[6] Lowe SL, Willis BA, Hawdon A, Natanegara F, Chua L, Foster J, Shcherbinin S, Ardayfio P and Sims JR. Donanemab (LY3002813) dose-escalation study in Alzheimer's disease. Alzheimers Dement (N Y) 2021; 7: e12112.

[7] Yue CM, Deng DJ, Bi MX, Guo LP and Lu SH. Expression of ECRG4, a novel esophageal cancer-related gene, downregulated by CpG island hypermethylation in human esophageal squamous cell carcinoma. World J Gastroenterol 2003; 9: 1174-1178.

[8] Gotze S, Feldhaus V, Traska T, Wolter M, Reifenberger G, Tannapfel A, Kuhnen C, Martin D, Muller O and Sievers S. ECRG4 is a candidate tumor suppressor gene frequently hypermethylated in colorectal carcinoma and glioma. BMC Cancer 2009; 9: 447.

[9] Li LW, Yu XY, Yang Y, Zhang CP, Guo LP and Lu SH. Expression of esophageal cancer related gene 4 (ECRG4), a novel tumor suppressor gene, in esophageal cancer and its inhibitory effect on the tumor growth in vitro and in vivo. Int J Cancer 2009; 125: 1505-1513.

[10] Xu PT, Li YJ, Qin XJ, Scherzer CR, Xu H, Schmechel DE, Hulette CM, Ervin J, Gullans SR, Haines J, Pericak-Vance MA and Gilbert JR. Differences in apolipoprotein E3/3 and E4/4 allele-specific gene expression in hippocampus in Alzheimer disease. Neurobiol Dis 2006; 21: 256-275.

[11] Kujuro Y, Suzuki N and Kondo T. Esophageal cancer-related gene 4 is a secreted inducer of cell senescence expressed by aged CNS precursor cells. Proc Natl Acad Sci U S A 2010; 107: 8259-8264.

[12] Podvin S, Miller MC, Rossi R, Chukwueke J, Donahue JE, Johanson CE, Baird A and Stopa EG. The Orphan C2orf40 gene is a neuroimmune factor in Alzheimer's disease. JSM Alzheimers Dis Relat Dement 2016; 3: 1020.

[13] Baird A, Coimbra R, Dang X, Lopez N, Lee J, Krzyzaniak M, Winfield R, Potenza B and Eliceiri BP. Cell surface localization and release of the candidate tumor suppressor Ecrg4 from polymorphonuclear cells and monocytes activate macrophages. J Leukoc Biol 2012; 91: 773-781.

[14] Lee J, Dang X, Borboa A, Coimbra R, Baird A and Eliceiri BP. Thrombin-processed Ecrg4 recruits myeloid cells and induces antitumorigenic inflammation. Neuro Oncol 2015; 17: 685-696.

[15] Moriguchi T, Kaneumi S, Takeda S, Enomoto K, Mishra SK, Miki T, Koshimizu U, Kitamura H and Kondo T. Ecrg4 contributes to the anti-glioma immunosurveillance through type-I interferon signaling. Oncoimmunology 2016; 5: e1242547.

[16] Mirabeau O, Perlas E, Severini C, Audero E, Gascuel O, Possenti R, Birney E, Rosenthal N and Gross C. Identification of novel peptide hormones in the human proteome by hidden Markov model screening. Genome Res 2007; 17: 320-327.

[17] Ozawa A, Lick AN and Lindberg I. Processing of proaugurin is required to suppress proliferation of tumor cell lines. Mol Endocrinol 2011; 25: 776-784.

[18] Gallwitz M, Enoksson M, Thorpe M and Hellman L. The extended cleavage specificity of human thrombin. PLoS One 2012; 7: e31756.

[19] Albert MS, DeKosky ST, Dickson D, Dubois B, Feldman HH, Fox NC, Gamst A, Holtzman DM, Jagust WJ, Petersen RC, Snyder PJ, Carrillo MC, Thies B and Phelps CH. The diagnosis of mild cognitive impairment due to Alzheimer's disease: recommendations from the national institute on aging-Alzheimer's association workgroups on diagnostic guidelines for Alzheimer's disease. Alzheimers Dement 2011; 7: 270-279.

[20] Menck K, Bleckmann A, Schulz M, Ries L and Binder C. Isolation and characterization of microvesicles from peripheral blood. J Vis Exp 2017; 55057.

[21] Waybright T, Avellino AM, Ellenbogen RG, Hollinger BJ, Veenstra TD and Morrison RS. Characterization of the human ventricular cerebrospinal fluid proteome obtained from hydrocephalic patients. J Proteomics 2010; 73: 1156-1162.

[22] Kizuka Y, Kitazume S, Fujinawa R, Saito T, Iwata N, Saido TC, Nakano M, Yamaguchi Y, Hashimoto Y, Staufenbiel M, Hatsuta H, Murayama S, Manya H, Endo T and Taniguchi N. An aberrant sugar modification of BACE1 blocks its lysosomal targeting in Alzheimer's disease. EMBO Mol Med 2015; 7: 175-189.

[23] Barres BA, Hart IK, Coles HS, Burne JF, Voyvodic JT, Richardson WD and Raff MC. Cell death in the oligodendrocyte lineage. J Neurobiol 1992; 23: 1221-1230.
[24] Donato R, Miljan EA, Hines SJ, Aouabdi S, Pollock K, Patel S, Edwards FA and Sinden JD. Differential development of neuronal physiological responsiveness in two human neural stem cell lines. BMC Neurosci 2007; 8: 36.
[25] Hide T, Takezaki T, Nakatani Y, Nakamura H, Kuratsu J and Kondo T. Sox11 prevents tumorigenesis of glioma-initiating cells by inducing neuronal differentiation. Cancer Res 2009; 69: 7953-7959.
[26] Takanaga H, Tsuchida-Straeten N, Nishide K, Watanabe A, Aburatani H and Kondo T. Gli2 is a novel regulator of Sox2 expression in telencephalic neuroepithelial cells. Stem Cells 2009; 27: 165-174.
[27] Thomas M and Klibanov AM. Enhancing polyethylenimine's delivery of plasmid DNA into mammalian cells. Proc Natl Acad Sci U S A 2002; 99: 14640-14645.
[28] Nishide K, Nakatani Y, Kiyonari H and Kondo T. Glioblastoma formation from cell population depleted of Prominin1-expressing cells. PLoS One 2009; 4: e6869.
[29] Folstein MF, Folstein SE and Mchugh PR. Mini-mental state - practical method for grading cognitive state of patients for clinician. J Psychiatr Res 1975; 12: 189-198.
[30] Kaufer DI, Williams CS, Braaten AJ, Gill K, Zimmerman S and Sloane PD. Cognitive screening for dementia and mild cognitive impairment in assisted living: comparison of 3 tests. J Am Med Dir Assoc 2008; 9: 586-593.
[31] Saxton J, Morrow L, Eschman A, Archer G, Luther J and Zuccolotto A. Computer assessment of mild cognitive impairment. Postgrad Med 2009; 121: 177-185.
[32] Hampel H, Shen Y, Walsh DM, Aisen P, Shaw LM, Zetterberg H, Trojanowski JQ and Blennow K. Biological markers of amyloid beta-related mechanisms in Alzheimer's disease. Exp Neurol 2010; 223: 334-346.
[33] Palmqvist S, Insel PS, Stomrud E, Janelidze S, Zetterberg H, Brix B, Eichenlaub U, Dage JL, Chai X, Blennow K, Mattsson N and Hansson O. Cerebrospinal fluid and plasma biomarker trajectories with increasing amyloid deposition in Alzheimer's disease. EMBO Mol Med 2019; 11: e11170.
[34] Karlsson M, Zhang C, Mear L, Zhong W, Digre A, Katona B, Sjostedt E, Butler L, Odeberg J, Dusart P, Edfors F, Oksvold P, von Feilitzen K, Zwahlen M, Arif M, Altay O, Li X, Ozcan M, Mardinoglu A, Fagerberg L, Mulder J, Luo Y, Ponten F, Uhlen M and Lindskog C. A single-cell type transcriptomics map of human tissues. Sci Adv 2021; 7: eabh2169.
[35] Temple S. Advancing cell therapy for neurodegenerative diseases. Cell Stem Cell 2023; 30: 512-529.
[36] Seo JH, Miyamoto N, Hayakawa K, Pham LD, Maki T, Ayata C, Kim KW, Lo EH and Arai K. Oligodendrocyte precursors induce early blood-brain barrier opening after white matter injury. J Clin Invest 2013; 123: 782-786.
[37] Niu J, Tsai HH, Hoi KK, Huang N, Yu G, Kim K, Baranzini SE, Xiao L, Chan JR and Fancy SPJ. Aberrant oligodendroglial-vascular interactions disrupt the blood-brain barrier, triggering CNS inflammation. Nat Neurosci 2019; 22: 709-718.
[38] Gonzalez AM, Podvin S, Lin SY, Miller MC, Botfield H, Leadbeater WE, Roberton A, Dang X, Knowling SE, Cardenas-Galindo E, Donahue JE, Stopa EG, Johanson CE, Coimbra R, Eliceiri BP and Baird A. Ecrg4 expression and its product augurin in the choroid plexus: impact on fetal brain development, cerebrospinal fluid homeostasis and neuroprogenitor cell response to CNS injury. Fluids Barriers CNS 2011; 8: 6.
[39] Municio C, Carrero L, Antequera D and Carro E. Choroid plexus aquaporins in CSF homeostasis and the glymphatic system: their relevance for Alzheimer's disease. Int J Mol Sci 2023; 24: 878.
[40] Depp C, Sun T, Sasmita AO, Spieth L, Berghoff SA, Nazarenko T, Overhoff K, Steixner-Kumar AA, Subramanian S, Arinrad S, Ruhwedel T, Mobius W, Gobbels S, Saher G, Werner HB, Damkou A, Zampar S, Wirths O, Thalmann M, Simons M, Saito T, Saido T, Krueger-Burg D, Kawaguchi R, Willem M, Haass C, Geschwind D, Ehrenreich H, Stassart R and Nave KA. Myelin dysfunction drives amyloid-beta deposition in models of Alzheimer's disease. Nature 2023; 618: 349-357.
[41] Blanchard JW, Akay LA, Davila-Velderrain J, von Maydell D, Mathys H, Davidson SM, Effenberger A, Chen CY, Maner-Smith K, Hajjar I, Ortlund EA, Bula M, Agbas E, Ng A, Jiang X, Kahn M, Blanco-Duque C, Lavoie N, Liu L, Reyes R, Lin YT, Ko T, R'Bibo L, Ralvenius WT, Bennett DA, Cam HP, Kellis M and Tsai LH. APOE4 impairs myelination via cholesterol dysregulation in oligodendrocytes. Nature 2022; 611: 769-779.

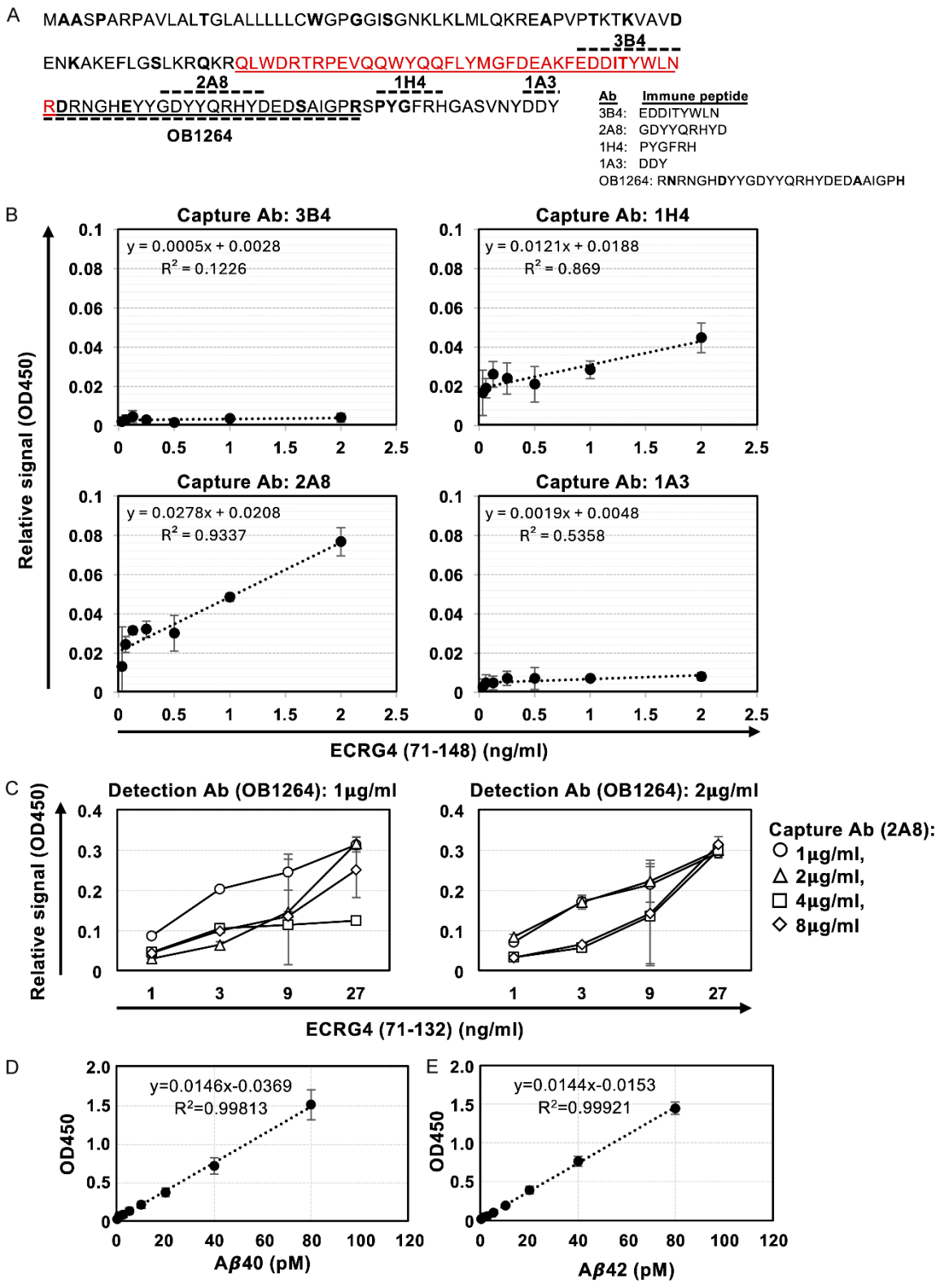

Figure S1. Development of an ECRG4 ELISA system. A. Information on immunized peptides (dashed line) related to the human ECRG4 AA sequence. OB1264 was generated using the mouse Ecrg4 peptide. The differences between mouse and human ECRG4 AA sequences are indicated in bold. Mouse and rabbit Abs are shown at the top and bottom of the AA sequence, respectively. The solid underline indicates the region of ECRG4 (71-132). ECRG4 (71-107)

as shown in red. B. Standard curves for detecting ECRG4 (71-148) using four combinations of capture Ab (3B4, 1H4, 2A8 or 1A3) and detection Ab (OB1264). Each symbol indicates the approximate curve. C. Standard curves for detecting ECRG4 (71-132) using OB1264 (1 or 2 μg/ml) and 2A8 (1 (circle), 2 (triangle), 4 (square) or 8 (diamond) μg/ml). D. Representative standard curve for detecting Aβ40. E. Representative standard curve for detecting Aβ42. Formulas indicate the approximate curves. Error bar: ± SD.

Table S1. Classification of dementia and Mild cognitive impairment (MCI) patients

Patient age (years old)		-40	41-50	51-60	61-70	71-80	81-
Dementia	Alzheimer's Disease (AD)	M: 1	M: 1, F: 1	M: 10, F: 4	M: 10, F: 13	M: 23, F: 35	M: 9, F: 23
	Normal pressure hydrocephalus (NPH)			M: 1	M: 1, F: 1	M: 3, F: 1	M: 1, F: 1
	Idiopathic NPH (iNPH)				M: 2		
	Progressive nonfluent aphasia (PNFA)				F: 1	F: 1	
	Progressive supranuclear palsy (PSP)				F: 1	F: 1	
	Dementia with Lewy bodies (DLB)				F: 1	M: 1	
	Frontotemporal lobar degeneration (FTLD)				M: 1		
	Vascular dementia (VaD)					F: 1	
	Neuronal intranuclear inclusion disease (NIID)					F: 1	
	Others	F: 1		M: 1, F: 1	M: 1, F: 1	M: 3, F: 4	
MCI				M: 1	M: 1, F: 6	M: 5, F: 10	M: 2, F: 2

Patients were categorized by diagnosis, gender (M: male, F: female) and age.

Table S2. Classification of non-dementia patients with neurological disorders

Patient age (years old)	-40	41-50	51-60	61-70	71-80	81-
Diagnosis	myospasm: M1, myoclonus: F1, migraine: F1, syringomyelia: F1, hysteria: M1, limbic encephalitis: M1, myopathy: M1, Neuromyelitis optica: M1, epilepsy: M1, aseptic meningitis: M1, F1, psychogenic reaction: F1, episodic ataxia: M1, sarcoidosis: M1, neuro-Behcet: F1, tuberculous meningitis: M1, femoral neuropathy: F1, multiple cerebral infarction: F1, multiple sclerosis: F1, post-resuscitation encephalopathy: F1, myelopathy: M1, fibromyalgia: F1	dystonia: F1, spastic paraplegia: M1, multiple system atrophy: F1, Huntington's disease: M1, encephalitis: M1, cervical dystonia: M1, Cervical cord sarcoidosis: M1, polymyositis: F1, diabetic peripheral neuropathy: M1, brachial neuritis: M1, neuro-Behcet: F1, immune-mediated neuropathy: M1, syringomyelia: F1, Cavernous vein sinus meninges: F1, hypothalamic lesion: F1	brachial plexus neuritis: M1, F1, thoracic myelopathy: M1, leukoencephalopathy: F1, aseptic meningitis: F1, paraneoplastic neurological syndrome: M1, cerebellar ataxia: M1, peripheral neuropathy: F1, muscular dystrophy:F1, myopathy: M1, spastic paraplegia: M1, encephalopathy: F1, cervical spondylotic myelopathy: F1	hypertrophic pachymeningitis: M1, multiple system atrophy: M2, multiple cranial nerve palsy: M1, myelitis: F1, Muscle sarcoidosis: F1, neurosarcoidosis: F1, Sequelae of myelitis: F2, limbic encephalitis: F1, cerebellar ataxia: M1, myelopathy: M2, spastic paraplegia: M1, alcoholic cerebellar atrophy: M1, corticobasal degeneration: F1, cerebral infarction sequelae: F1, Left lower limb weakness: M1, late-onset hypogonadism syndrome: M1	spondylosis deformans: F1, Pure akinesia: F1, Sensory neuropathy: F1, multiple system atrophy: M1, myelitis: M1, dural arteriovenous fistula: F1, inclusion body myositis: M1	spastic paraplegia: M1, Multiple cranial nerve disorders: F1, motor neuron disease: F1, cranial polyneuritis: F1

Table S3. Primer lists

PCR fragment	the 5' primer	the 3' primer
Esophageal cancer related gene 4 (Ecrg4) (32-70)	TGATATCGAACAAACTCAAGAAGATGCTCC	AAGATCTTCGTTTGGCACGCTTCAGG
Ecrg4 (71-132)	TGATATCGCAGCTGTGGGACCGTACG	AAGATCTGTGGGGACCAATGGCCGCA
Ecrg4 (133-148)	ATCGAGCCGGGAAAGCTTCAGGCATGGAGCCAGTGTCAACTATAATGACTATA	GATCTATAGTCATTATAGTTGACACTGGCTCCATGCCTGAAGCTTTCCCGGCTCGAT
Solute carrier family 46 member 3 (SLC46A3)	ACCACATTTTGGGGAGCTTG	AGCCAGATGACAGTCCTGTT
Carbohydrate sulfotransferase 3 (CHST3) (Human)	GCAGGGCAACATCTTCTACC	CACAGGAAGAGCTGCTTGAG
Chst3 (rat)	CAGAAGGCCCGAGAGATGTA	AACTGCTCCGAGGAGTTCTT
Tetratricopeptide repeat domain 39A (TTC39A)	CACACTTTCGAATCCAGGCA	TCCAGCTGTCTCTGTCTTCC
18S	CGGACAGGATTGACAGATTG	CAAATCGCTCCACCAACTAA

Underline restriction enzyme site.

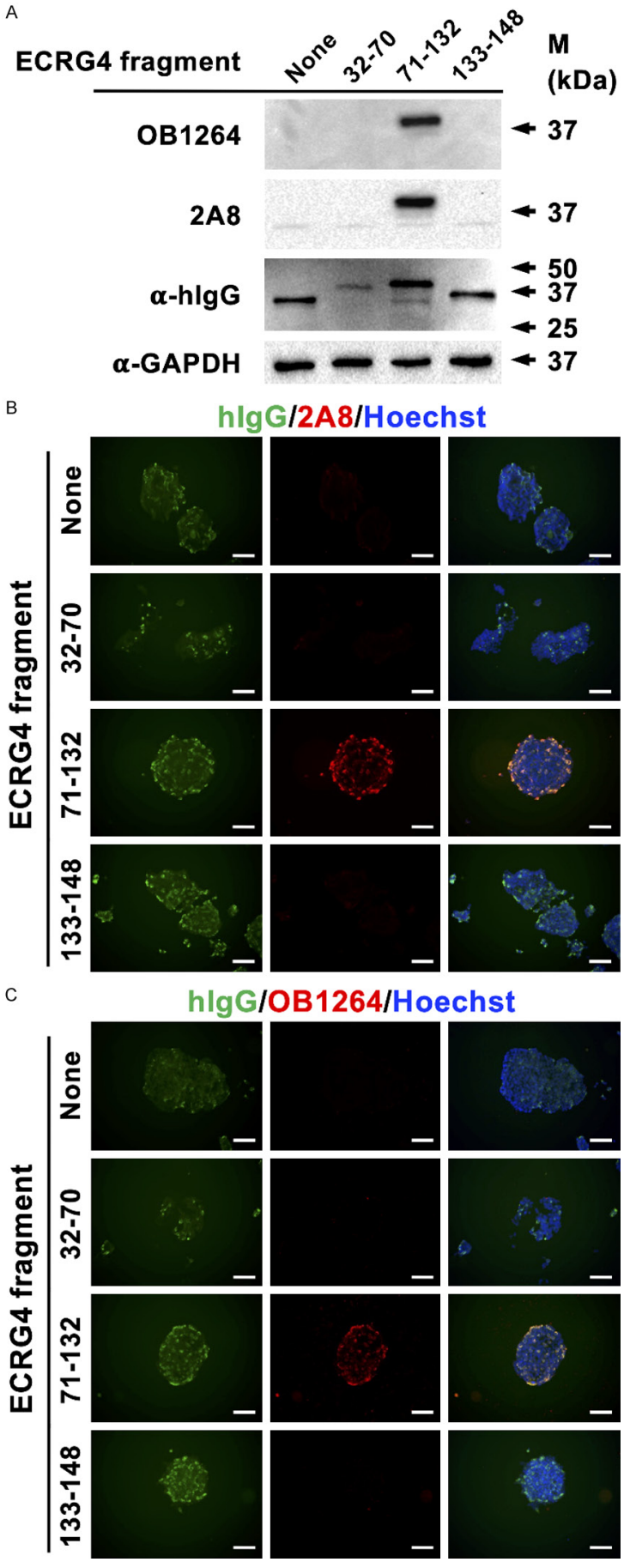
A
ECRG4 fragment
None
32-70
71-132
133-148
M (kDa)
OB1264
2A8
α-hIgG
α-GAPDH
37
37
50
37
25
37
B
hIgG/2A8/Hoechst
ECRG4 fragment
None
32-70
71-132
133-148
C
hIgG/OB1264/Hoechst
ECRG4 fragment
None
32-70
71-132
133-148

Figure S2. Specificity of mouse and rabbit anti-ECRG4 Abs. (A) A set of Ecrg4-hIgG expression vectors (32-70, 71-132 and 133-148) and the parental vector (None) were transfected into 293T cells. Cell extracts were harvested three days after transfection and then analyzed by Western blotting using anti-ECRG4 (OB1264 and 2A8), anti-hIgG and anti-GAPDH (loading control) antibodies. Figure displayed cropped blots of each data. (B, C) Representative photographs of transfected 293T cells with the Ecrg4-hIgG expression vectors immunostained with anti-Ecrg4, 2A8 (B, red) and OB1264 (C, red) along with anti-hIgG (green). All nuclei were counterstained with Hoechst 33342 (blue). Scale bar: 100 μm.

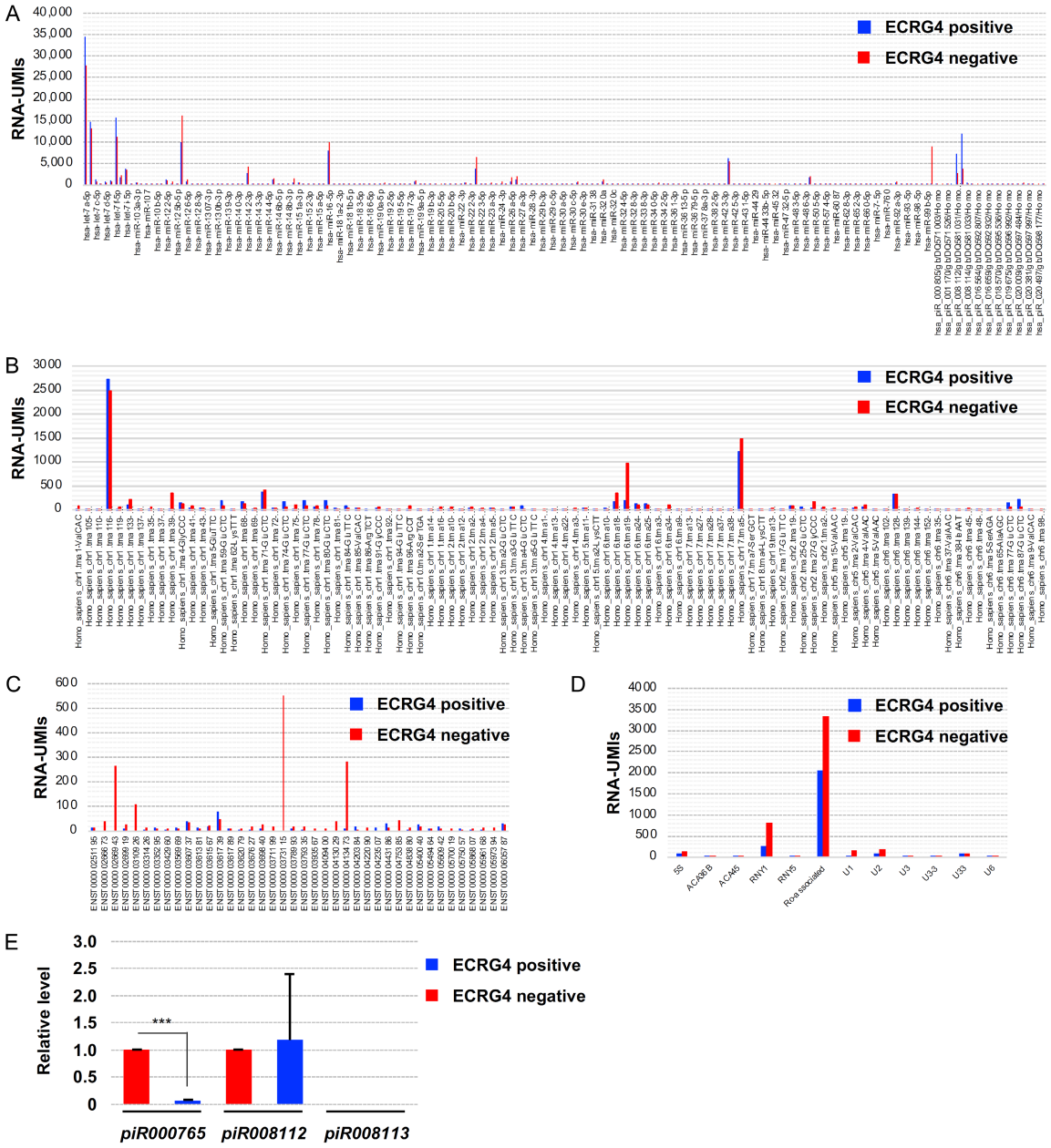

Figure S3. RNA sequencing analysis of mixed plasma from ECRG4-positive and -negative AD patients. A. Levels of miRNA and piRNA in the plasma of patients. B. Levels of tRNA in the plasma of patients. C. Levels of mRNA in the plasma of patients. D. Levels of other RNA in the plasma of the patients. E. Relative levels of three candidate piRNAs, piR000765, piR008112 and piR008113 in ECRG4-positive and -negative serums. The expression was normalized using let7b as an internal control. Statistical significance was determined by the t test. ***P < 0.001. UMIs: Unique Molecular Identifiers. ECRG4-positive and -negative plasma samples are presented in blue and red, respectively.

Table S4. Spearman correlation coefficients among variables in plasma samples (N = 267)

Variables	Sex	ECRG4	Aβ40	Aβ42	Aβ42/Aβ40	Age
Sex ρ	-	-0.045	0.017	-0.009	-0.008	-0.118
p (two-tailed)	-	0.466	0.781	0.889	0.891	0.054
ECRG4 ρ	-0.045	-	-0.437***	-0.455***	-0.305***	0.152*
P	0.466	-	< 0.001	< 0.001	< 0.001	0.013
Aβ40 ρ	0.017	-0.437***	-	0.703***	0.15*	0.103
P	0.781	< 0.001	-	< 0.001	0.014	0.092
Aβ42 ρ	-0.009	-0.455***	0.703***	-	0.751***	0.084
P	0.889	< 0.001	< 0.001	-	< 0.001	0.172
Aβ42/Aβ40 ρ	-0.008	-0.305***	0.15*	0.751***	-	-0.011
P	0.891	< 0.001	0.014	< 0.001	-	0.863
Age ρ	-0.118	0.152*	0.103	0.084	-0.011	-
P	0.054	0.013	0.092	0.172	0.863	-

Significance, *$P < 0.05$, ***$P < 0.001$.

Table S5. Spearman correlation coefficients among variables in CSF samples (N = 200)

Variables	Sex	ECRG4	Aβ40	Aβ42	Aβ42/Aβ40	Age
Sex ρ	-	-0.061	-0.103	-0.211**	-0.164*	0.13
p (two-tailed)	-	0.387	0.147	0.003	0.021	0.066
ECRG4 ρ	-0.061	-	0.032	0.024	0.04	-0.049
P	0.387	-	0.657	0.732	0.576	0.488
Aβ40 ρ	-0.103	0.032	-	0.673***	-0.016	-0.203**
P	0.147	0.657	-	< 0.001	0.818	0.004
Aβ42 ρ	0.211**	0.024	0.673***	-	0.675***	0.259***
P	0.003	0.732	< 0.001	-	< 0.001	< 0.001
Aβ42/Aβ40 ρ	0.164*	0.04	-0.016	0.675***	-	-0.136
P	0.021	0.576	0.818	< 0.001	-	0.055
Age ρ	0.13	-0.049	-0.203**	0.259***	-0.136	-
P	0.066	0.488	0.004	< 0.001	0.055	-

Significance, *$P < 0.05$, **$P < 0.01$, ***$P < 0.001$.

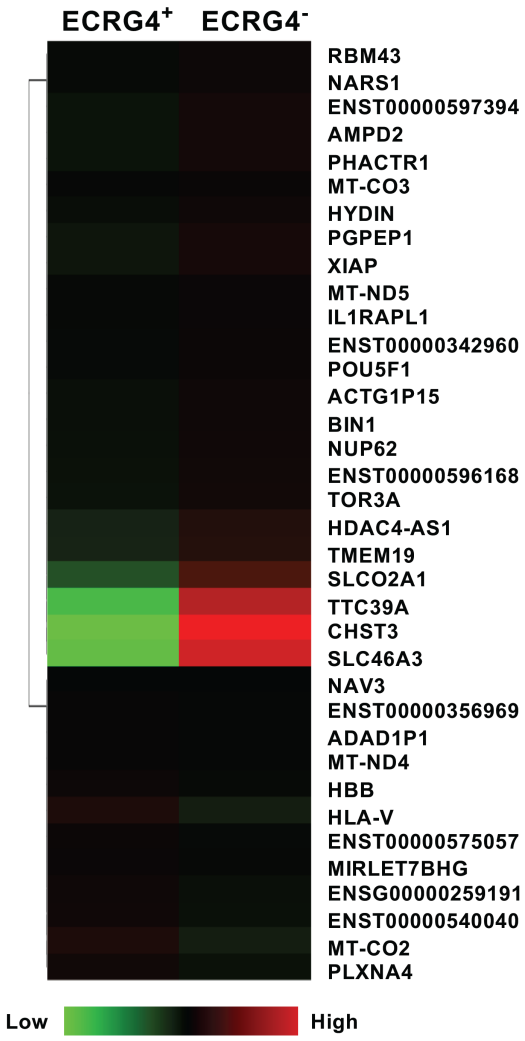

Figure S4. iDEP analysis of the RNA sequencing data. Hierarchical clustering identified three genes, TTC39A, CHST3, and SLC46A3, which were decreased in the serum of ECRG4^{+} patients compared to that of ECRG4^{-} patients.